NOAA TECHNICAL MEMORANDUM ERL PMEL-109

WESTERLY WIND EVENTS IN THE TROPICAL PACIFIC, 1986–1995: AN ATLAS FROM THE ECMWF OPERATIONAL SURFACE WIND FIELDS

G.A. Vecchi[1]
D.E. Harrison[2]

[1] Joint Institute for the Study of Atmosphere and Ocean (JISAO)
University of Washington
Seattle, WA 98195

[2] Pacific Marine Environmental Laboratory
7600 Sand Point Way N.E.
Seattle, WA 98115-0070

May 1997

Contribution No. 1810 from NOAA/Pacific Marine Environmental Laboratory

NOTICE

Mention of a commercial company or product does not constitute an endorsement by NOAA/ERL. Use of information from this publication concerning proprietary products or the tests of such products for publicity or advertising purposes is not authorized.

Contribution No. 1810 from NOAA/Pacific Marine Environmental Laboratory

For sale by the National Technical Information Service, 5285 Port Royal Road
Springfield, VA 22161

CONTENTS

Page

Abstract 1
1. Introduction 1
2. Data 3
3. Methods 4
3.1 Classification 4
3.2 Compositing 5
4. Composite Results 6
4.1 Vector maps 6
4.2 Center day wind maps 8
4.3 Scales 9
5. WWEs and the TOGA-COARE Intensive Observations Period 10
6. Temporal Distribution 11
6.1 Single event distributions 11
6.2 Multi-event distributions 12
7. Summary and Discussion 13
8. Acknowledgments 15
9. References 15
APPENDIX: Statistical Significance Methods 19
TABLES 23
FIGURES 37

Westerly Wind Events in the Tropical Pacific, 1986–1995: An Atlas from the ECMWF Operational Surface Wind Fields

G.A. Vecchi[1] and Harrison, D.E.[2]

Abstract. We present an atlas of results from an analysis of Westerly Wind Events (WWEs) in 10 years of the European Centre for Medium Range Weather Forecasting (ECMWF) 10-m wind field analysis. We compare the analysis wind field to the Comprehensive Ocean-Atmosphere Data Set (COADS) climatology and to wind time series from the Tropical Atmosphere-Ocean (TAO) array. We present a classification scheme for the westerly wind variability we observe in the data, using eight types based on the location of the maximum westerly winds. We construct a composite for each type of event, and show the results for a 21-day composite period for each one, both for winds and anomalies. A simple propagating Gaussian model satisfactorily describes the evolution of zonal wind anomaly for each type of event; we estimate the scales of each composite event by fitting the model to each composite. Several instances of wide-spread westerly wind anomaly are identified and described, but these "mega"-WWEs have few features in common. We discuss the WWEs that occurred during the Tropical Ocean and Global Atmosphere (TOGA) Coupled Ocean-Atmosphere Response Experiment (COARE) Intensive Observing Period (IOP) and show the extent to which our composite events are able to reproduce the major westerly wind features of the IOP. We describe the frequency of occurrence of each type of WWE for each year of this record and by monthly climatology; we find that several types of events are negatively correlated with the annual mean Troup Southern Oscillation Index (SOI), and that the stronger WWEs often have a statistically significant seasonality. We believe that our composites offer a useful framework for representing the sort of westerly wind variability that occurs in the western and central tropical Pacific and can provide a basis for further study of the importance of such winds in the climatological and interannual variability of this part of the world ocean. However, we note that this decade was dominated by years in which the SOI was negative; reliable frequency statistics and SOI correlations may require a longer analysis period.

1. Introduction

The existence of unusual multi-day periods of surface westerly winds over the western and central tropical Pacific was noted during the planning for the Tropical Ocean and Global Atmosphere (TOGA) program. Some of the most striking instances of these events occur when tropical cyclones pair on either side of the equator (Keen, 1982); but westerly wind variability is much more common than are paired cyclones (Luther et *al*., 1983; Harrison and Geise, 1991; Hartten, 1996). Harrison and Geise (1991) used 30 years of near-date line island surface wind observations (1950–1980) to characterize the meridional and time scales of westerly wind events (WWEs) seen at these islands. They suggested that near-date line WWEs could be classified into four relatively distinct types according to distance from the equator of the strongest westerly wind anomaly. They also noted a significant tendency for near-date line WWEs to be associated preferentially with warm El Niño-Southern Oscillation (ENSO) periods and with particular seasons. The limited spatial coverage of the island data set was inadequate to provide a full characterization of the events.

[1] Joint Institute for the Study of Atmosphere and Ocean (JISAO), University of Washington, Seattle, WA 98195
[2] NOAA, Pacific Marine Environmental Laboratory, 7600 Sand Point Way NE, Seattle, WA 98115-0070

The large-scale circulation structures associated with WWEs are of interest. Harrison (1984) showed that a dramatic southerly flow which began over the Tasman Sea (40°S) and later crossed the Equator, immediately preceded the onset of strong equatorial westerly winds at the beginning of the 1982–83 ENSO warming period. Others have provided additional examples of a subtropical association to particular equatorial westerly winds, as well as a tendency for cross equatorial flow from the winter hemisphere to precede the formation of some tropical westerly anomalies (Love, 1985a; Chu, 1988; Chu and Frederick, 1990). Hartten (1996) describes an effort to update and extend the analysis of Harrison and Geise (1991) to the entire western tropical Pacific, with particular attention to large-scale aspects of the circulation associated with periods of westerly winds. According to her subjective classification scheme for westerly wind bursts (WWBs), 90% of the synoptic westerly wind variability in the western Pacific can be described using one of nine categories.

It is our goal to extend our knowledge about WWEs and their space and time scales. We think this is now possible because much work has been devoted to improving the operational surface meteorological analyses in the tropics. Since 1986 the U.S. Navy, U.S. National Centers for Environmental Prediction (NCEP) (NOAA), and the European Centre for Medium Range Weather Forecasting (ECMWF) have each developed improved tropical surface wind analyses. Further, the TOGA-TAO array has been providing, particularly since about 1992, substantially larger amounts of quality surface wind data as input to the analyses than have ever before been available. The TAO array was fully deployed for the first time in late 1994.

This atlas presents the day-to-day evolution of our WWE composites, as well as an extensive collection of other statistics pertaining to WWEs over this decade. Harrison and Vecchi (1997) only show selected results from our analyses. This atlas, together with the discussion of Harrison and Vecchi (1997), offers a complete look at our results.

After considerable evaluation, we consider the ECMWF surface wind analysis now to be sufficiently plausible to provide a basis for this study. We have used it to prepare a description of the x-y-t characteristics of WWEs during the period 1986–1995. Section 2 describes the data sets used; section 3 describes our screening process and the compositing technique we have used in this study. We present our composite results and describe a simple mathematical model structure for these composite WWEs in section 4. The westerly wind variability during the TOGA-Coupled Ocean-Atmosphere Response Experiment (COARE) Intense Observation Period (IOP) and the ability of our composite events to characterize the IOP variability is presented in section 5. Section 6 discusses the seasonal and interannual distribution of WWEs and their correlation with the Southern Oscillation Index, and describes the extent to which WWEs occur in particular sequences. Section 7 offers some summary and discussion.

2. Data

We used as our wind data set the ECMWF 10-m operational 12-hourly wind analysis, on their 2.5° × 2.5° global grid. Our attention was on the region from 100°E to 100°W, by 30°S to 30°N and over the years 1986–1995. The ECMWF analysis was significantly improved in the middle 1980s, hence our choice of 1986 for the beginning of this analysis effort. Other changes to their operational analysis were implemented after 1986, but we found no dramatic changes in the fields sufficient to deter us from this project. We constructed a monthly climatology from the 12-hourly ECMWF surface wind analysis of the entire 10 years of record (1986–1995), using a time axis centered on the mid-day of each month. We defined our anomalies as the difference between the instantaneous wind and the climatology, linearly interpolated in time.

In order to assess the utility of the ECMWF 10-m wind field, we carried out two comparisons. First we looked at the large time and space scale aspects of the circulation, and compared our ECMWF monthly climatology to a Comprehensive Ocean-Atmosphere Data Set (COADS) (Woodruff *et al.*, 1987) monthly climatology from 1946 through 1993. Then we examined the short time-scale variability by comparing ECMWF time series with data from the TOGA-TAO buoys (McPhaden, 1993).

Figures 1–6 show the comparison of the ECMWF with the COADS monthly climatologies for zonal wind. Figures 7–12 show the comparison of the ECMWF with the COADS climatologies for meridional wind. Figures 13–18 show the comparison of the ECMWF and the COADS climatologies for wind divergence. For all these plots the COADS climatology is smoothed with a 5-point triangle filter (half power point at 18°) in the zonal direction and a 3-point triangle smoother (half power point at 11°) in the meridional direction. We find no large-scale differences in the zonal and meridional wind field of large enough amplitude to affect the results of this study (see Harrison and Vecchi, 1997).

The March and September divergence patterns for the ECMWF and COADS climatologies are compared in Figs. 13–18. The two climatologies have similar divergence patterns, with maximum convergence in the ITCZ and the South Pacific Convergence Zone (SPCZ). Generally the location and meridional scale of each convergence zone are similar, but the ECMWF convergence is substantially weaker than COADS. We see no large-scale differences in the central and western tropical Pacific sufficient to merit concern.

We computed the RMS difference between the daily averaged ECMWF wind analysis, interpolated to each buoy location (when necessary), and the daily averaged buoy winds. No trends were removed. Note that the period over which it was possible to compute the RMS difference varies from buoy to buoy, so there can be significant change from one longitude to another. The buoys along 110°W, 140°W, and 165°E had the longest time series; other buoys had data for as little as a year, because they were recently deployed. The results for a large sampling of the buoys are presented in Fig. 19. Overall, the zonal and meridional wind results were comparable. Maximum RMS differences were about 2.5 and minimum differences about 1 m s^{-1}. The largest values tended

to be in the ITCZ and SPCZ regions, although the differences along 165°E were 2 m s^{-1} or more from 5°N to 9°S. The smallest values tended to be in the eastern SE trade winds.

The implication of these values comes following comparison with the magnitude of the WWE signal (which we later shall show is 8 to 20 m s^{-1}) and with the accuracy of the TAO measurement. The wind sensors themselves are claimed to be accurate to about 0.2 m s^{-1} pre-deployment and are estimated to drift by up to 0.5 m s^{-1} during 1 year of activity (Mangum *et al.*, 1994). It should also be noted that the wind measurements on the buoys are done at 4 m from the surface, while the ECMWF winds are at 10 m. According to a stability correction algorithm developed by W.G. Large (Large and Pond, 1981) to adjust wind speed from a height *z* to a height of 10 m, we found that the wind speed correction is typically 10% or less. Thus without height adjustment we may expect errors of about 0.5 m s^{-1} on a wind of 5 m s^{-1} or 1 m s^{-1} for 10 m s^{-1} wind. Since we cannot height-adjust the TAO winds because the information required to make the stability correction is typically not available, we suggest a plausible expected mean error on the TAO data to be 0.7 to 1.5 m s^{-1} under typical moderate WWE conditions. Thus the disagreement between the TAO data and the ECMWF data is similar to the uncertainty in the TAO data; and, since WWEs typically have maximum zonal winds in excess of 10 m s^{-1}, use of the ECMWF analysis gives us an acceptable signal-to-noise ratio.

3. Methods

3.1. Classification

We began by looking at vector plots of the wind and wind anomalies over the tropical Pacific for every 12-hour analysis period in our data set. Based on the wind anomaly patterns we saw, we defined eight regions to serve as the framework for our classification scheme. These regions, which cover most of the ocean from 120°E to 150°W and 15°S to 15°N, were named according to their location relative to each other. The zonal dimension of these regions is about 30° of longitude, and the meridional dimension is 10° of latitude. Each contains five ECMWF grid points in the meridional direction, and twelve to thirteen points in the zonal direction. To help the viewer place them in the context of the large-scale environment of the region, we show the regions superimposed upon the COADS climatological (1946–1995) mean winds, SST, and SLP for 12 calendar months (Figs. 20–31).

In order to systematically identify and analyze WWEs, we introduced a quantitative definition for their existence, within the context of our classification scheme. We defined a WWE of type ***X*** as any period of 3 or more days for which the 10-m zonal wind anomaly, averaged over region ***X*** and smoothed by a three-point triangle filter in time (half-power point at 2.75 days), exceeded 2 m s^{-1}. To label and organize the events, an event's center day was defined to be the day for which the zonal wind anomaly, averaged over the region, was greatest. With these classification criteria we identified all the westerly wind events by region (type) and center date.

We find it useful to describe the intensity of the WWEs according to their "duration," "maximum averaged anomaly," "maximum point anomaly," and "wind measure." We defined the

duration of each WWE to be the time span between when the identification criteria are first met and when the identification criteria are no longer satisfied. We defined the maximum averaged anomaly to be the zonal wind anomaly averaged over the classifying region on the center day of the event. The maximum point anomaly is the maximum zonal wind anomaly within the classifying region on the center date. We defined the wind measure as the time integral of the zonal wind anomaly, averaged within the classifying region and smoothed by a three-point triangle filter in time (half-power point at 2.75 days), over the event duration.

Not every period of westerly wind anomalies fit perfectly into our classification scheme. In particular, sometimes substantial westerly wind anomalies occurred in adjacent regions at the same time. This led us to make an additional sub-classification of WWEs into overlapping and non-overlapping events. We defined overlapping events to be events which were identified in two regions that shared more than half an edge and whose center dates were within 3 days of each other. For each pair of overlapping events, we compared the maximum averaged anomaly for each event, and classified the event as an event of the type for which the maximum averaged anomaly was greatest. We then had two lists of dates, one with all the events, which we shall refer to as the "complete event list," and another with all the non-overlapping events plus the overlapping events classified according to our secondary classification scheme, which we will refer to as the "non-overlapping event list." We identified 351 events in the complete event list: 58–NW, 28–N, 36–E, 35–W, 62–C, 42–E, 39–S, and 51–SE. We identified 287 events in the non-overlapping event list: 51–NW, 25–N, 28–E, 28–W, 49–C, 34–E, 29–S, and 43–SE. Table 1 shows the complete event list arranged by center date, along with the identifying region, duration, maximum averaged anomaly, maximum point anomaly, and wind measure.

3.2. Compositing

The basis of our compositing is the identification of the center day (day (0)) for each event of a type "X". We compute the day(0) field for our composite type "X" event by averaging together the wind or wind anomaly field for all the type "X" event days(0). Composite day(±n) is computed similarly from each of the days(±n) for type "X" events. We evaluate the composite for day(–10) through day(10) for each of the eight types of WWEs, resulting in a 21-day composite event. The composites are evaluated using all the events from each type of WWE.

For each type of event, then, our composite is evaluated according to:

$$\vec{U}(x,y,t_n) = \frac{\sum_{i=1}^{N} \vec{u}(x,y,t_n+\tau_i)}{N}$$

Where $\vec{U}$ is the composite vector wind anomaly, $\vec{u}$ is the instantaneous vector wind anomaly, x is the zonal location, y is the meridional location, $\{\tau_i\}$ are the center days for the individual events, $\tau_n \in [-9,10]$ is the event day, and N is the number of events to be composited. To study the effect of

overlap in the averaging process, we generated two sets of composite westerly wind events: one using the dates in the complete event list, the other using the dates in the non-overlapping event list. The two composites were not different in any significant qualitative aspect. Thus we present only the composites generated from the complete event list. Also, we similarly computed the composite wind fields for each type of event.

4. Composite Results

4.1. Vector maps

We computed daily wind anomaly vector maps for days (–10) through (10) for each of the eight types of WWEs (Figs. 32–87). Note in these figures that the region used to define the featured type of event is outlined. The anomalies highlighted as bold vectors have zonal component significant at the 99% level, and those highlighted by a shaded background have meridional wind component comparably significant. Statistical significance was determined by a Student's-*t* test (Appendix).

We describe qualitatively the features of the patterns that seem to us to merit note, and follow the atmospheric convention that an easterly wind is a wind from the east, etc. It is helpful to introduce composite wind magnitude labels as follows: weak ($u \leq 2$ m s^{-1}), moderate (2 m s^{-1} < $u \leq 4$ m s^{-1}) and strong ($u > 4$ m s^{-1}). We find it is simplest to identify common elements in the composite events by sorting them into Northern Regions (NW, N, and NE), the Equatorial Regions (W, C, and E), and the Southern Regions (S and SE).

4.1.1. Northern regions: NW, N, and NE (Figs. 32–38, 39–45, and 46–52)

Each of these events has strong meridional and zonal wind anomalies. Although the areas of maximum significance are principally occupied by moderate to strong westerly and southwesterly anomalies, there are clear suggestions that these events are associated with anomalously cyclonic circulations, with moderate to strong easterlies and northerlies to the north and west of the regions. All of these events also show a modest translation of the area of maximum anomalies during the event. The type N and NW events show northwestward displacement throughout the event, while the type NE event shows an eastward displacement throughout the event.

The NW and N type events share additional common features. Both types of events have periods of distinct weak to moderate cross-equatorial inflow from day(–3) until day(2) for the type NW event, and from day(–3) until day(0) for the type N event. There is also well-defined inflow from west of the cyclonic feature from day(–2) to day(3) for the type NW event, and from day(–2) to day(2) for the type N event. The circulation is more complicated than a simple cyclonic flow.

The NW and NE type events share periods of weak to moderate equatorial westerly anomalies. For the NW type events, there is a period of equatorial westerlies to the south of the classifying region prior to the center day, lasting 8 days, centered around day(–5), when the maximum equatorial westerly occurs; there are also weak equatorial westerlies from day(2) through day(5),

to the southeast of the region. For the type NE events, equatorial westerlies to the south of the classifying region occur during the period of maximum anomaly in the region, last for 3 days and have their peak amplitude on the center day of the event.

4.1.2. Equatorial regions: W, C, and E (Figs. 53–59, 60–66 and 67–73)

For each of the equatorial WWEs the maximum anomalies are primarily zonal, with periods of moderate meridional inflow to the western part of the regions. The equatorial westerlies in all three events are meridionally contained within the defining region, but their zonal extent can be substantially larger than the defining region. The meridional inflow typically can be found at least 20 degrees away from the equator, but can extend as far as 30 degrees (the southerly inflow on day(0) of the type C event). For the type C composite event, the zonal wind anomalies are close to symmetric with respect to the Equator, while for the types W and E event there is a pronounced asymmetry. The type W composite event has symmetric anomalies in the early part of its evolution, while as day(0) is approached the anomalies become more pronounced to the north of the Equator. The type E composite event has its largest anomalies to the south of the Equator.

For the type W event there is moderate southerly inflow during event days(–5) and (–4), followed by a moderate northerly inflow that begins on the center day, and an anomalous cyclonic circulation subsequently develops. For the type C event there is moderate northerly and southerly inflow beginning on day(–1) and ending after day(1). For the type E event, there is moderate southerly inflow beginning on day(–2) that continues until the center day. Both the type W and the type E events exhibit a translation of the area of maximum anomaly. The W type event has a translation towards the northwest after the center day. The type E event has a westward translation after the center day.

4.1.3. Southern regions: S and SE (Figs. 74–80 and 81–87)

Both of these composite events have a moderate to strong meridional component as well as strong westerly anomalies near day(0). Although most of the significant anomalies are westerly and northwesterly, there are also moderate to strong easterly and southerly anomalies suggesting a pattern of anomalously cyclonic flow. The events also exhibit eastward translation of the area of maximum anomaly throughout the event.

Both of the composite events exhibit moderate cross-equatorial inflow on and immediately preceding the center day. The cross-equatorial inflow for the type S event occurs through the northwestern corner of the region as well as the eastern half of the northern edge of the region, from day(–2) through day(0). For the type SE event, the cross-equatorial flow is most persistent north of the eastern corner of the region, from day(–2) through day(0). Both events exhibit strong inflow from the west on the days before and during the period of maximum anomaly. The westerly inflow for the type S event begins on day(–9) and extends as far west as the Indian Ocean. So the structure

of the circulation of these events, like that of the type N and NW events, is not just a simple cyclonic one.

The type SE event has persistent weak to moderate equatorial westerly anomalies on the days surrounding the center day. The equatorial westerlies are stronger to the south of the equator than to the north of it. The type SE event also has moderate southerly inflow from higher latitudes on the days preceding and on the center day.

4.2. Center day wind maps

Figures 88–143 show vector plots of the center day of the total wind composite, for each type of WWE. As before, it is helpful to discuss the composites by grouping the events by northern, equatorial, and southern regions.

4.2.1. Northern regions: NW, N, and NE (Figs. 88–94, 95–101, and 102–108)

The anomalously cyclonic circulations in the type NW and N anomaly composites manifest themselves as cyclonic wind patterns in our wind composites. The type N wind pattern indicates a reversal of the northeasterly trades within the classifying region. The situation differs for the type NE event, for which the wind composite indicates a trade wind break, but not a cyclonic wind pattern, because of the strength of the northeasterly trades in that region. The translation of the area of maximum anomaly noted in the anomaly plots is also apparent in the full sequence of wind composite figures.

The cross-equatorial inflow noted in the type NW and N event anomalies is also apparent in the wind composites, but the anomaly inflow from the west is not clear in the winds themselves. The equatorial westerly anomalies in the type NW event appear as actual equatorial westerly winds to the south of the region. The equatorial westerly anomalies noted in the type NE events do not appear as equatorial westerly winds here.

4.2.2. Equatorial regions: W, C, and E (Figs. 109–115, 116–122, and 123–129)

For the type W and C events, the primarily zonal westerly anomalies in the region appear as primarily zonal westerly winds. However, for the type E event, the wind field has a noticeable meridional component. Also, while the anomalies for the type C event were centered about the equator, the winds are asymmetrical with the greatest westerly amplitudes south of the equator (this is due to the seasonality of the strong type C event, which tend to occur in austral winter when the climatological winds south of the equator are westerly). The equatorial asymmetry of the type E zonal wind anomalies is also noticeable in the wind composite.

The southerly inflow anomaly in the type W and C events appears as a strengthening of the already prominent southeasterly trade winds to the east of Australia. For the type E event, southerly inflow is apparent, and is linked to a cyclonic circulation pattern to the southwest of the region, which translates westward. For the type W event the northerly inflow anomaly is discernible in the

winds; so is the cyclonic anomaly circulation which tends to move northwestward. For the type C event the northerly inflow anomaly is overwhelmed by the strong trade winds, but a cyclonic wind circulation forms, centered to the south of the region, which does not propagate from day(–4) when it first appears to day (4) when it dissipates.

4.2.3. Southern regions: SE and S (Figs. 130–136, and 137–143)

Both of these composite events display strong meridional winds, as well as zonal winds in the classifying regions. The type SE composite winds shows a reversal of the southeasterly trades. The winds also have a cyclonic pattern to them, which translates to the east as it decays for the type S events, and decays quickly for the type SE event. The cross-equatorial inflow anomaly for the type S event produces cross-equatorial flow in the winds. For the type SE event, there is no cross-equatorial flow in the area of cross-equatorial anomalies. For the SE type event the anomalously southerly inflow enhances the southeasterly trade winds to the west of the trade wind reversal.

4.3. Scales

Now we turn to the problem of defining the scales of our composite WWEs. Table 2 shows the duration, maximum averaged anomaly, wind measure, and maximum point anomaly for each of the composite WWEs. The events have a duration in the range of 4.5–5.5 days, except the type NE event (4 days). The maximum averaged anomaly is in the range of 3.9 to 4.7 m s^{-1}; the strongest events are type SE (4.7 m s^{-1}) and type N (4.6 m s^{-1}), and the weakest is type W (3.9 m s^{-1}). The wind measure for all the events is between 1.1 and 1.6 × 10^6 m; the strongest event is type N (1.6 × 10^6 m). The events have maximum point anomaly between 6.3–7.2 m s^{-1}, except the type E event (5.5 m s^{-1}).

Histograms for duration, maximum point anomaly, maximum averaged anomaly, and wind measure for all the events over the entire record are shown in Fig. 144. Histograms for these quantities are shown by region in Figs. 145–148. The effects of the smoothing in compositing are evident for the maximum point anomaly if Table 2 is compared with Figs. 145–148, while from the same comparison one notices that for the more large-scale quantities (maximum averaged anomaly, duration, and wind measure) the smoothing effects are small.

To characterize the behavior of the zonal wind anomaly field as simply as possible, we formulated a simple analytical model for it. We constructed *x*-*t* and *y*-*t* contour plots of the zonal wind anomaly for each type of event (Figs. 149–156), and found the zonal wind anomaly to be sharply bounded in space and time.

We use a Gaussian in (*x*,*y*,*t*) with translating center to define the scales of our events:

$$U(x,y,t_n) = U_o \exp\left\{-\left[\frac{x - X_o + c_x t}{L_x}\right]^2\right\} \exp\left\{-\left[\frac{y - Y_o + c_y t}{L_y}\right]^2\right\} \exp\left\{-\left[\frac{t_n}{T}\right]\right\}$$

Where U is the model zonal wind anomaly field, U_o is the maximum point anomaly, (X_o,Y_o) is the geographic center, (c_x,c_y) is the translational velocity, (L_x,L_y) are the spatial e-folding scales, T is the temporal e-folding scale, and x, y, and t_n are as in section 3. We then computed the scales for our Gaussian model and summarize them in Table 3.

5. WWEs and the TOGA-COARE Intensive Observations Period

The TOGA-COARE Intensive Observations Period (IOP) (Webster and Lukas, 1992; Lukas *et al*., 1995) offers an example period (November 1992–February 1993) when WWEs were the focus of a major oceanographic and meteorological field program. The IOP occurred during the warm phase of ENSO; ISOs passed over the western Pacific during the program (Chen and Houze, 1996; Lin and Johnson, 1996), and there were some tropical cyclones as well (McBride *et al*., 1995). So conditions were very favorable for the appearance of WWEs.

Table 4 lists the WWEs that occurred during the IOP according to our classification scheme. There were three type NE and C events, two type NW, N, E, and SE events, and one type W and S events during the IOP. Maximum point anomalies are $\geq$15 m s^{-1} in six events, between 10 and 15 m s^{-1} in nine events and less that 10 m s^{-1} in one event. The maximum averaged anomaly offers another indicator of the overall intensity of the event. By this standard the 1 Jan 1993 type S (10.4 m s^{-1}) and the 2 Jan 1993 type C (6.4 m s^{-1}) events are the most intense of the IOP. The next most intense are the 19 Nov 1992 type NE and the 6 Feb 1993 type SE events. The remaining events have maximum averaged anomalies of 5 m s^{-1} or less.

The final column of Table 4 lists the wind measure of each event, as defined in section 3. Three "primary" events have wind measure values near 4×10^6 m, four "secondary" events have values between 2.5×10^6 m and 3×10^6 m, and the rest have values less than or equal to 1.3×10^6 m. The three primary events are the type S and C events centered on 1 and 2 Jan 1993, and the type SE event centered on 6 Feb 1993. The secondary events are the type NW event centered on 20 Nov 1992, the type SE event centered on 3 Jan 1993, the type NE event centered on 5 Jan 1993 and the type C event centered on 31 Jan 1993. Late December 1992 and early January 1993 was the period of primary WWE activity according to the wind measure. The next most active period was late January 1993 through early February 1993.

These WWE statistics are consistent with westerly wind periods that have been discussed elsewhere. Eldin *et al*. (1994) reported strong westerly winds and found large eastward surface currents from their ship track along 156°E, during early January 1993 and early February 1993. The large westerly wind activity during early January 1993 and during early February 1993 coincided both times with the passage of the convectively active phase of an ISO (Lin and Johnson, 1996; Chen and Houze, 1996). Three WWEs seem to be associated with named tropical cyclones: the 31 Oct 1992 type N event (cyclones Dan and Carrie), the 20 Nov 1992 type NW event (cyclone Hunt), the 6 Feb 1993 type SE event (cyclone Mick) (McBride *et al*., 1995).

How well do our composite WWEs describe the periods of WWEs during the IOP? We have compared the IOP anomaly fields with the wind anomaly fields obtained by simply superimposing the composite anomaly WWEs for the events listed in Table 4. Figures 157–177 summarize these results. We find a number of instances in which the simple composite anomaly field is a good first approximation to the real anomaly field, and several instances where the simple field is not so satisfactory. Generally the composite description is more diffuse than the daily wind anomaly fields; amplitudes are somewhat reduced and length scales are somewhat larger, even in the defining regions. Outside the defining regions there can be substantial differences, but in the defining regions the wind anomalies are substantially smaller than in the defining regions. There is one situation in the IOP when the composite does not reproduce the basic features of the wind within the defining region, the type E event centered on 6 Feb 1993. This is also the weakest event during the IOP, based on the wind measure, and its maximum averaged anomaly is only barely over the identification threshold of 2 m s^{-1}. We find that some IOP off-equatorial events have less equatorial westerly wind than one would expect from the composite WWEs.

6. Temporal Distribution

6.1. Single event distributions

Consider first the climatological distribution by month. Figure 178 shows, for each region, the 10-year (1986–95) total number of WWEs that occurred during each calendar month. No striking variation is seen in the month-by-month comparison, but there is a clear seasonal preference for types NW, N, and S, which is statistically significant to the 99% level using the test described in the Appendix. A seasonal description for the distribution of the type NW WWEs is that of an "on" season from July through October, two transition seasons (May–June and November–December) and an "off" season from January through April. For the type N and S WWEs the simplest seasonal description is that of a 6-month "on" season and a 6-month "off" season. The "on" seasons are July through December for the type N event, and December through May for the type S event. We cannot define an "on" or "off" season for type NE, W, C, E, or SE events that is statistically significant at the 90% level.

The distribution of moderate or stronger WWEs is somewhat more striking; defining a moderate or stronger event as an event whose wind measure exceeds 2×10^6 m, leads to Fig. 179. Boreal summer and fall are the primary seasons for the type NW (July–December) and N (July–October) events; November through January is the primary season for type C events; and boreal winter and spring are the primary seasons for type S (December–April) and SE (December–March) events. While the type C events are evenly distributed across the months, most of the events that occur between November and February are of moderate or greater strength. All these seasonal distributions are significant to the 97% level. No seasonal distribution, significant even at 70%, exists for the strong type NE, W, and E events.

Now consider the year-to-year distribution of WWEs. Figure 180 shows the number of each type event, year by year from 1986 through 1995. The mean number of events is indicated by the thick horizontal line. It is also instructive to compare these distributions with the Troup Southern Oscillation Index (SOI). The 12-month running mean of (–1) × SOI is plotted along with the mean (–1) × SOI for the 10-year period 1986–95, as the lower left hand panel of Fig. 180. SOI values have been negative much of this period, indicating warm (ENSO) conditions for the tropical Pacific; the 10-year average is –4.5.

We see that the fewest number of events occurred in 1988 for every type of event, and in most regions 1989 was also a year of few events. 1988–89 was the only period of persistently positive SOI in this record. There is no comparably strong connection between years of negative SOI and more than normal total number of WWEs. However, lagged correlations between the SOI and the number of events in each region revealed that some statistically significant relationships exist. The strongest correlation (–0.85) exists for type C events at zero lag, and is 99% significant. Zero lag correlations significant at the 95% level exist for type NE (–0.69), E (–0.69) and SE (–0.68) events. Type NW and W regions have 90% significance level correlation (–0.61 and –0.59 respectively) but they lead the SOI by 1 year. Overall, then, we find that WWEs in our easternmost three regions and our C region are negatively correlated with zero lag to SOI. WWEs in our westernmost regions are negatively correlated at a 1-year lead with SOI. Only type N and S events do not show a significant correlation with SOI.

There is another WWE-SOI relationship of interest, which is evident in Figs. 181–184. In these figure we have plotted a scatter plot of the wind measure (Fig. 181), duration (Fig. 182), maximum averaged anomaly (Fig. 183), and maximum point anomaly (Fig. 184) for all events in our 10-year record. There is a clear relation between the periods with negative SOI and the event intensity indicators.

6.2. Multi-event distributions

We have emphasized the independence of WWEs throughout this study. Typically WWEs form, develop, and decay without any strong relationship with other events. We base this on having studied the sequencing of events with center days within 3 days of each other, looking to determine if there were any statistically significant patterns. In a few instances of substantial statistical significance (99%) different types of WWEs seem to be related. We find 18% of the time a type N event will evolve into a type NW event (5 times), 17% of the time a type W event will evolve into a type NW event (6 times) and 18% of the time a type S event will evolve into a type SE event (7 times). These three relationships are consistent with the translation speed of the original event. It must be noted that it is not typical for the second event to form out of the first. Two other statistically significant relationships exist in our record, for which we cannot propose mechanisms. In our record 18% of the time a type N event will precede a type SE event (5 times) and 14% of the time a type E event precedes a type NE event (6 times). These last relationships might be

coincidental, or there might be some mechanism which accounts for their occurrence. Longer records containing additional WWEs are needed to determine the robustness of these relationships; only a very few instances exist in out 10-year record.

Another aspect of interest in the frequency distribution of westerly winds was identified by computing the average zonal wind anomaly over the area spanned by all eight of our WWE regions. Recall that we define a WWE to exist in any one of our WWE regions when the area average zonal wind anomaly exceeds 2 m s^{-1} for 3 days. If we define a "Mega"-WWE (MWWE) to exist when the average over all eight regions meets the WWE criterion, we find there are eleven MWWEs in our analysis period. Figure 185 provides a cartoon of the spatial structure and wind measure of each MWWE.

The number of MWWEs by year is: 2–86, 1–90, 1–91, 3–92, 2–93, 2–94; MWWEs only occur during years when the annual average SOI was negative. We find a suggestion of seasonality in the meridional frequency of the component WWEs in each MWWE. The five MWWEs for which the dominant component WWEs were northern hemisphere WWEs occurred between the middle of August and the beginning of November; the three MWWEs which had southern hemisphere WWEs as their primary component WWEs all occurred between January and May; the three MWWEs which had equatorial WWEs as their main component WWEs occurred between late November and late April. However there are too few MWWEs for us to do meaningful statistics.

7. Summary and Discussion

We have examined ECMWF 10 m surface wind analyses every 12 hours between 1986 and 1995, to try to characterize the space and time scales of westerly wind events (WWEs) in the tropical Pacific Ocean. We found that Pacific WWEs can be classified satisfactorily according to the region in which they attain their maximum zonal wind anomalies, and that eight adjoining regions are needed to describe the different WWEs that we saw in the wind fields.

We generated a composite event for each type by averaging and find that the zonal wind anomalies associated with each type of event are quite compact in space and time. We modeled the structure of each event as a uniformly translating Gaussian in space and time. The typical amplitude is between 6 and 7 m s^{-1}; the typical *e*-folding time scale is about 3 days (duration is 6 days between the times of e^{-1} amplitude). The time-scales found by Harrison and Geise (1991) are longer (5–10 day), but the amplitudes obtained in this study compare well to theirs. The meridional *e*-folding scale varies between event types from 400 km to 1100 km, but values are mostly in the 600–700 km range; these meridional *e*-folding scales are slightly larger than those found by Harrison and Geise (1991). Zonal *e*-folding scales vary from 1400 km to 2500 km, while the equatorial events have *e*-folding scales of 1700 to 1900 km; Geise and Harrison (1991) estimated a zonal length scale of 20°, that is an *e*-folding scale of about 1000 km, from the island wind data. Some events translate slowly (largest speed is about 5 m s^{-1}) and others show no significant translational motion.

Our classification method is similar to an extension of that used by Harrison and Geise (1991), except that we have a two-dimensional surface wind field that covers the entire western and central Pacific, instead of a distribution of islands. We can extend our analysis to the zonal scales and translation characteristics of WWEs throughout the entire tropical Pacific.

Occasionally, much of the area spanned by our eight regions experiences westerly wind anomalies of sufficient intensity that the average over the entire area satisfies our criteria for the existence of a WWE. We call such events "mega"-WWEs (MWWEs). Eleven MWWEs occurred in our time period and we describe their features in section 4.1. No particular geographical distribution of WWEs was found in these MWWEs. However, a slight indication of seasonality for these events was found, with the MWWEs whose main events were off-equatorial preferentially occurring in the local summer and fall. MWWEs did not occur while the Troup-SOI was positive.

Composites like these are most useful when they reasonably well represent the characteristics of typical events in their region. The TOGA-COARE Intensive Observing Period (IOP) provided a 4-month period (November 1992–March 1993) which contained at least one event of each of our types. We described the WWEs of the IOP period in Table 4. There were 16 WWEs during the IOP; the events with the largest wind measure values occurred late December 1992, early January 1993, and toward the end of January 1993. Another period that was strongly forced was the third week of November 1992. Nine IOP events had wind measure less than 1.3×10^6 m, and seven of the events had wind measure greater than 2.5×10^6 m. Most events had maximum point anomaly values between 11 and 16 m s^{-1}; one event had maximum point anomaly greater than 19 m s^{-1} and one less than 10 m s^{-1}. There was a MWWE in early January 1993, involving four different types of WWEs (S, C, SE, and NE) in rapid sequence (center days between 1 Jan 1993 and 5 Jan 1993); this was one of the most intense periods of westerly wind variability in our 10-year record. The strong WWEs occurring at the beginning of January 1993 and the beginning of February 1993 were associated with the convectively active phase of an ISO (Lin and Johnson, 1996; Chen and Houze, 1996). Three WWEs were associated with named tropical cyclones, two in the northern hemisphere and one in the southern hemisphere.

We compared the wind anomaly fields produced simply by superimposing our composite anomalies in place of the particular WWEs of the IOP. In many cases the composite representation is reasonable. The most common shortcoming is that the weaker WWEs during the IOP typically were of shorter duration than our composites, particularly near the equator. This means that the composite representation tended to have more near-equatorial westerlies than the IOP wind anomalies indicate. It is not simple to characterize the events that are not well modeled by our composites; some had a small wind measure and others a large one, and there were no event types which were dramatically better (or worse) represented by their composite.

We also examined the distribution of WWEs with year, with climatological month and with Troup Southern Oscillation Index (SOI). Moderate to strong events (those with wind measure greater than 2×10^6 m) show distinct seasonality for some WWE types, with off-equatorial events

tending to favor local summer and fall seasons, and type C events tending to favor boreal winter, while no seasonality is apparent in either the type NE, W, or E events. These seasonal distributions are consistent with those found by Harrison and Geise (1991) and by Hartten (1996). Correlation of annual distribution with SOI is less simply summarized, in part because the SOI was predominantly negative during our period of study—only mid-1988 through mid-1989 and late 1995 had SOI persistently positive. Overall we find 95% statistically significant negative correlation between SOI and type C, NE, E, and SE events at zero lag, and 90% significant negative correlation between SOI and type NW and W events with the events leading the SOI by a year. The type C event is the only event whose correlation with Troup SOI is significant to the 99% level.

WWEs are an unusual mode of tropical atmospheric variability. According to this analysis the off-equatorial events are almost always associated with tropical cyclonic systems (not to be confused with named tropical cyclones), but the period in which substantial westerly wind anomalies exist over regions of any significant extent is not characterized by strong translation of the cyclonic system. In four of our off-equatorial composite WWEs (types NW, N, S, and SE) we find moderate (2–4 m s^{-1}) cross-equatorial inflow as well as moderate (2–4 m s^{-1}) inflow from the west during the days surrounding the center day (see section 4.1.).

The near-equatorial WWEs are sometimes, but not always, associated with cyclonic circulations on either (or both) hemisphere. In many instances events of these types appear to be simple down-gradient pressure flows, with meridional scale determined by the atmospheric first radius of deformation. The near-equatorial events in our analysis seem also to have a mid-latitude connection, with cross-equatorial inflows similar to those described by Love (1985a), Chu (1988), and Chu and Frederick (1990). We find moderate to strong (>2 m s^{-1}) meridional inflows generating poleward of 20° on the days preceding and on the center day of the event.

8. Acknowledgments

This work was carried out with support from NOAA's Pacific Marine Environmental Laboratory, ERL Headquarters and Office of Global Programs (support to the Stanley P. Hayes Center at the University of Washington) and from NASA. This is PMEL Contribution #1810 and JISAO Contribution #1745. DEH wishes to thank Gene Rasmusson for his interest and encouragement to study what we now call WWEs, more than 15 years ago. The help of the TMAP group at PMEL is also gratefully acknowledged. Mom, Dad, Dan, and Eva.

9. References

Bickel, P.J., and K.A. Doksum (1977): *Mathematical Statistics: Basic Ideas and Selected Topics*. Holden-Day, Inc., 492 pp.

Chen, S.S., R.A. Houze, Jr., and B.E. Mapes (1996): Multiscale variability of deep convection in relation to large-scale circulation in TOGA COARE. *J. Atmos. Sci.*, *53*(10), 1,380–1,409.

Chu, P.S. (1988): Extratropical forcing and the burst of equatorial westerlies in the western Pacific: A synoptic study. *J. Met. Soc. Japan, 66*(4), 549–564.

Chu, P.S., and J. Frederick (1990): Westerly wind bursts and surface heat fluxes in the equatorial western Pacific in May 1982. *J. Met. Soc. Japan, 68*(5), 523–536.

Delcroix, T., G. Eldin, M. McPhaden, and A. Morliere (1993): Effects of westerly wind bursts upon the western equatorial Pacific Ocean, February–April 1991. *J. Geophys. Res., 98*, 16,379–16,385.

Eldin, G., T. Delcroix, C. Hénin, K. Richards, Y. Du Penhoat, J. Picaut, and P. Rual (1994): Large-scale current and thermohaline structures along 156°E during the COARE Intensive Observation Period. *Geophys. Res. Lett., 21*(24), 2681–2684.

European Centre for Medium Range Weather Forecasts (19??): The description of the ECMWF/WCRP level III—A global atmospheric data archive, technical attachment, 72 pp.

Geise, B.S. (1989): Equatorial oceanic response to forcing on time scales from days to months. NOAA Technical Memorandum ERL PMEL-87 (NTIS PB89-206775), 99 pp.

Geise, B.S., and D.E. Harrison (1990): Aspects of the Kelvin wave response to episodic wind forcing. *J. Geophys. Res., 95*(C5), 7289–7312.

Geise, B.S., and D.E. Harrison (1991): Eastern equatorial Pacific response to three composite westerly wind types. *J. Geophys. Res., 96*(sup), 3239–3248.

Gill, A.E. (1982): *Atmosphere-Ocean Dynamics*. Academic Press, 662 pp.

Harrison, D.E. (1984): On the appearance of sustained equatorial westerlies during the 1982 Pacific warm event. *Science, 225*, 1,099–1,102.

Harrison, D.E., and P.S. Schopf (1984): Kelvin-wave induced anomalous advection and the onset of surface warming in El Niño events. *Mon. Wea. Rev., 112*(5), 923–933.

Harrison, D.E., and B.S. Geise (1988): Remote westerly wind forcing of the eastern equatorial Pacific: some model results. *Geophys. Res. Lett., 15*, 804–807.

Harrison, D.E., and D.S. Luther (1990): Surface winds from tropical Pacific islands—Climatological statistics. *J. Clim., 3*(2), 251–271.

Harrison, D.E., and B.S. Geise (1991): Episodes of surface westerly winds as observed from islands in the western tropical Pacific. *J. Geophys. Res., 96*, 3221–3237.

Harrison, D.E., and N. Larkin (1996): The COADS sea level pressure signal: A near-global El Niño composite and time series view, 1946–1993. *J. Clim., 9*(12), 3025–3055.

Harrison, D.E., and N. Larkin (1997): The ENSO surface temperature and wind signal: A near-global composite and time-series view, 1946–1995. *Rev. Geophys.*, submitted.

Harrison, D.E., and G.A. Vecchi (1997): Westerly wind events in the tropical Pacific, 1986–1995. *J. Clim.*, accepted.

Hartten, L.M. (1996): Synoptic settings of westerly wind bursts. *J. Geophys. Res., 101*(D12), 16,997–17,019.

Joint Typhoon Warning Center (1994a): Western North Pacific Typhoons—1994. *Mar. Wea. Log, 38*(1), 34–40.

Joint Typhoon Warning Center (1994b): Western North Pacific Typhoons—1993. *Mar. Wea. Log, 38*(4), 16–23.

Keen, R.A. (1982): The role of cross-equatorial cyclone pairs in the Southern Oscillation. *Mon. Wea. Rev., 110*, 1405–1416.

Kiladis, G.N., G.A. Meehl, and K.M. Weickmann (1994): Large-scale circulation associated with westerly wind bursts and deep convection over the western equatorial Pacific. *J. Geophys. Res., 99*(D9), 18,527–18,544.

Kindle, J.C., and P.A. Phoebus (1995): The ocean response to operational wind bursts during the 1991–1992 El Niño. *J. Geophys. Res., 100*(C3), 4,803–4,920.

Large, W.G., and S. Pond (1981): Open ocean momentum flux measurments in moderate to strong winds. *J. Phys. Oceanogr., 11*, 324–336.

Lau, K.H., and N.C. Lau (1992): The energetics and propagation dynamics of tropical summertime synoptic-scale disturbances. *Mon. Wea. Rev., 120*, 2,523–2,539.

Lau, K.M., L. Peng, C.H. Sui, and T. Nakazawa (1989): Dynamics of super cloud clusters, westerly wind bursts, 30–60 day oscillations and ENSO: A unified view. *J. Meteorol. Soc. Japan, 67*(2), 205–219.

Lin, X., and R.H. Johnson (1996): Kinematic and thermodynamic characteristics of the flow over the western Pacific warm pool during TOGA COARE. *J. Atmos. Sci., 53*(5), 695–715.

Livezey, R.E., and W.Y. Chen (1983): Statistical field significance and its determination by Monte Carlo techniques. *Mon. Wea. Rev., 111*, 47–59.

Love, G. (1985a): Cross-equatorial influence of winter hemisphere subtropical cold surges. *Mon. Wea. Rev., 113*, 1,487–1,498.

Love, G. (1985b): Cross-equatorial interactions during tropical cyclogenesis. *Mon. Wea. Rev., 113*, 1,499–1,509.

Lukas, R., P.J. Webster, M. Ji, and A. Leetma (1995): The large-scale context for the TOGA coupled ocean-atmosphere response experiment. *Meteorol. Atmos. Phys., 56*, 3–16.

Luther, D.S., D.E. Harrison, and R.A. Knox (1983): Zonal winds in the central equatorial Pacific and El Niño. *Science, 222*, 327–330.

Madden, R.A., and P.R. Julian (1972): Description of global-scale circulation cells in the tropics with a 40–50 day period. *J. Atmos. Sci., 29*, 1,109–1,123.

Madden, R.A., and P.R. Julian (1994): Observations of the 40–50 day tropical oscillation—A review. *Mon. Wea. Rev., 122*, 814–837.

Mangum, L.J., H.P. Freitag, and M.J. McPhaden (1994): TOGA-TAO array sampling schemes and sensor evaluations. *Proc. of the Oceans '94 OSATES*, vol. II, 402–406.

McBride, J.L., N.E. Davidson, K. Puri, and G.C. Tyrell (1995): The flow during TOGA COARE as diagnosed by the BMRC tropical analysis and prediction system. *Mon. Wea. Rev., 123*, 717–736.

McPhaden, M.J. (1993): TOGA-TAO and the 1991–93, El Niño-Southern Oscillation Event. *Oceanography, 6*(2), 36–44.

McPhaden, M.J., F. Bahr, Y. Du Penhoat, E. Firing, S.P. Hayes, P.P. Niiler, P.L. Richardson, and J.M. Toole (1992): The response of the western equatorial Pacific Ocean to westerly wind bursts during November 1989 to January 1990. *J. Geophys. Res., 97*, 14,289–14,303.

Meehl, G.A., G.N. Kiladis, K.M. Weickmann, M. Wheeler, D.S. Gutzler, and G.P. Compo (1996): Modulation of equatorial subseasonal convective episodes by tropical-extratropical interaction in the Indian and Pacific Ocean regions. *J. Geophys. Res., 101*(D10) 15,033–15,049.

Rasmusson, E.M., and T.H. Carpenter (1982): Variations in tropical sea surface temperature and surface wind fields associated with the Southern Oscillation/El Niño. *Mon. Wea. Rev., 110*, 354–384.

Rui, H., and B. Wang (1990): Development characteristics and dynamic structure of tropical intraseasonal convection anomalies. *J. Atmos. Sci., 47*, 357–379.

Schopf, P.S., and D.E. Harrison (1983): On equatorial Kelvin waves and El Niño, I, Influence of initial states on wave-induced current and warming. *J. Phys. Oceanogr., 13*, 936–948.

Spiegel, M.R. (1994): *Theory and Problems of Statistics*. Schaum's Outline Series, McGraw-Hill Inc.

Sui, C.H., and K.M. Lau (1992): Multiscale phenomena in the tropical atmosphere over the western Pacific. *Mon. Wea. Rev., 120*(3), 407–430.

Tsutsui, J., and A. Kasahara (1996): Simulated tropical cyclones using the National Center for Atmospheric Research community climate model. *J. Geophys. Res., 101*(D10), 15,013–15,032.

Webster P.J., and R. Lukas (1992): TOGA COARE: The Coupled Ocean-Atmosphere Response Experiment. *Bull. Am. Meteorol. Soc., 73*(9), 1377–1416.

Woodruff, S.D., R.J. Slutz, R.L. Jenne, and P.M. Steurer (1987): A comprehensive ocean-atmosphere data set. *Bull. Am. Meteorol. Soc., 68*, 1239–1250.

Wyrtki, K. (1975): El Niño—The dynamic response of the equatorial Pacific Ocean to atmospheric forcing. *J. Phys. Oceanogr., 5*, 572–584.

Zhang, C. (1996): Atmospheric variability at the surface in the tropical western Pacific Ocean. *J. Atmos. Sci., 53*(5), 739–758.

Zwillinger, D. (1996): *CRC—Standard Mathematical Tables and Formulae*, 30th Ed., CRC Press, 812 pp.

APPENDIX

Statistical Significance Methods

a. Composite wind anomaly significance test

We use a Students-*t* test to estimate the statistical significance of our composite results, so we require the standard deviation of the zonal and meridional wind anomalies that make up each composite. In particular, we needed to know these standard deviations for every 12-hour period during the 19 days of the composite. These standard deviations were computed as follows:

$$\vec{s}\left(x,y,t_n\right)=\left\{\frac{\sum_{i=1}^{N}\left[\vec{U}\left(x,y,t_n\right)-\vec{u}\left(x,y,\tau_i+t_n\right)\right]^2}{N-1}\right\}^{1/2}$$

where $\vec{s}$ is the standard deviation vector, $\vec{U}$, $\vec{u}$, x, y, t_n, $\{\tau_i,\}$ and N are the same as in section 3.1, and we define a vector to the power of α to be:

$$\vec{\xi}\equiv\begin{pmatrix}\xi_1\\ \xi_2\end{pmatrix}\Rightarrow\vec{\xi}^{\,a}\equiv\begin{pmatrix}\xi_1^a\\ \xi_2^a\end{pmatrix}$$

We performed a Student's-*t* test (Bickel and Docksun, 1977, p. 210–215) on each component of our composite vector wind anomaly field, to determine whether the true mean was distinguishable from zero, to the 99% confidence limit. We use a double-sided significance test, since we are interested in wind components that are statistically significant, regardless of the sign. We set the number of degrees of freedom in our test to be the number of individual events that went into generating the composite minus 1, using previous notation: N–1. According to the Student's-*t* test, our averages were significant to the 99% level if the following inequality was satisfied:

$$\left|\frac{\vec{U}\left(x,y,t_n\right)}{\vec{s}\left(x,y,t_n\right)}\right|>\frac{t_{99\%,\,N-1}}{\sqrt{N}}$$

Where, $\vec{U}$, $\vec{s}$, x, y, t_n, and N are as before; $\hat{e}_j$ is the unit vector in the zonal (j = 1) or meridional (j = 2) direction; $t_{99\%,N}$ is the double-sided Student's-*t* coefficient at the 99% significance level for N–1 degrees of freedom; and $\vec{\xi}\cdot\vec{\eta}$ indicates the vector dot product operation. The values for $t_{99\%,N}$ are tabulated in most statistics or mathematical table handbooks, e.g., Speigel (1994), Zwillinger (1996).

b. Correlation coefficient significance test

We performed a Student's-*t* (Bickel and Docksun, 1977, p. 220) test on our sample correlation coefficients, r, to evaluate whether the true correlation coefficient, ρ, approximated r was distinguishable from zero, to a prescribed significance level, l. We use a double-sided significance

test because we are interested in significant correlations regardless of the sign of the correlation. The following inequality had to be satisfied in this test:

$$r^2 > \frac{t^2_{1,N-2}}{N-2+t^2_{1,N-2}}$$

where $t_{l,N-2}$ is the double-sided Student's-*t* coefficient for *l* significance level and for *N*–2 degrees of freedom. Since in our case $N = 10$, the threshold for 95% significance is $|r| > 0.63$, and the threshold for 99% significance is $|r| > 0.77$, for the zero lag correlation tests; while for the 1-year lagged case $N = 9$, the threshold for 90% significance is $|r| > 0.58$, and for 95% significance $|r| > 0.67$. The values for $t_{l,N-2}$ are tabulated in most statistics or mathematical table handbooks, e.g., Speigel (1994), Zwillinger (1996).

c. Monthly distribution significance test

We performed a Monte Carlo test (Livezey and Chen, 1983) on the monthly distribution data to find the probability, *P*, that an "on" season had of occurring randomly in a sample from a uniform random distribution. We then took the significance level of the seasonal distribution to be $100 \times (1–P)\%$. The probability was computed using a Monte Carlo method, with 100,000 Monte Carlo samples.

The procedure to determine the probability of N_{seas} events being distributed over a continuous L_{saes} month period on a random distribution of *N* events is as follows. We sample 100,000 times; at each sampling we randomly distribute the *N* events for the particular event type, into 12 equally likely months. We then test whether there exists a continuous period of L_{seas} months for which the total number of events randomly placed is equal to or greater than N_{seas}. We count the number of times the test turns out true in our Monte Carlo procedure, and define the Monte Carlo probability to be $P = E/B$; where *E* is the number of positive tests, and *B* is the number of Monte Carlo samples. The Monte Carlo probability converged for $B > 1{,}000$, but we took $B = 100{,}000$ for good measure.

d. Event sequencing significance test

We performed a Monte Carlo test (Livezey and Chen, 1983) to find the probability, *P*, the sequencing pattern we observed for each event pair had of occurring randomly. We then took the significance level of the event sequencing to be $100 \times (1–P)\%$. The probability was computed using a Monte Carlo method, with 10,000 Monte Carlo samples.

We determined the probability of distributing N_1 center days of type 1 and N_2 center days of type 2 on a 10-year time axis semi-randomly, so that no two center days of the same type were within 7 days of each other, and having *M* or more ordered pairs of events (n_1,n_2) within 3 days of each other, in the following manner. We sample 10,000 times, at each sampling step semi-randomly distributing N_1 and N_2 events as just described. We then test to see how many ordered pairs (n_1,n_2) are within 3 days of each other. We count the number of times the test turns out true in our Monte

Carlo procedure, and define the Monte Carlo probability to be $P = E/B$; where E is the number of positive tests, and B is the number of Monte Carlo samples. The Monte Carlo probability converged for $B > 1{,}000$, but we took $B = 10{,}000$ for good measure.

TABLES

Table 1. Listing of all the events identified in the ECMWF wind data, from 1986 to 1995. Events are ordered according to their center date. See text for description of the quantities.

Center Date	Classifying Region								Duration (Days)	Maximum Averaged Anomaly ($m\ s^{-1}$)	Maximum Point Anomaly ($m\ s^{-1}$)	Wind Measure (10^6 m)
	NW	N	NE	W	C	E	S	SE				
25 Jan 86			NE						7	3.1	5.3	1.6
25 Jan 86							S		4.5	4.7	12.0	1.3
30 Jan 86								SE	3	3.6	8.0	0.8
4 Feb 86	NW								4.5	4.5	13.1	1.4
8 Feb 86							S		8.5	4.6	8.8	2.5
8 Feb 86								SE	11	5.0	11.6	4.0
13 Feb 86			NE						6	4.1	9.9	1.7
12 Apr 86							S		4.5	3.6	8.4	1.2
15 Apr 86			NE						6.5	4.1	11.4	1.7
12 May 86								SE	4.5	4.4	11.6	1.2
14 May 86	NW								5	3.0	8.9	1.2
17 May 86					C				5.5	4.8	12.5	1.4
19 May 86		N							4.5	4.6	15.8	1.2
19 May 86				W					11	4.7	7.6	3.1
22 May 86	NW								7.5	4.9	10.4	2.2
24 May 86		N							3	3.3	5.4	0.7
28 Jun 86	NW								4	3.0	5.3	0.9
1 Jul 86		N							4	3.7	9.7	0.9
3 Jul 86								SE	4.5	4.2	10.4	1.2
4 Jul 86	NW								4	2.7	7.7	0.8
18 Jul 86		N							15	4.1	6.7	3.8
31 Jul 86					C				3	2.4	4.8	0.6
31 Jul 86	NW								9	5.3	9.2	2.9
7 Aug 86								SE	4.5	6.0	11.8	1.6
14 Aug 86								SE	5	5.3	8.7	1.4
19 Aug 86						E			3	3.7	5.5	0.7
21 Aug 86		N							16.5	7.4	14.0	7.2
23 Aug 86	NW								16	6.3	13.3	5.5
1 Sep 86	NW								3.5	4.4	8.7	0.9
10 Sep 86				W					5.5	4.1	8.1	1.5
15 Sep 86	NW								3.5	4.0	10.9	1.0

Table 1. (Continued)

Center Date	Classifying Region								Duration (Days)	Maximum Averaged Anomaly (m s^{-1})	Maximum Point Anomaly (m s^{-1})	Wind Measure (10^6 m)
	NW	N	NE	W	C	E	S	SE				
22 Sep 86		N							6	5.8	10.8	2.0
23 Sep 86						E			5	4.2	6.4	1.4
28 Sep 86					C				4	4.0	6.7	1.1
30 Sep 86								SE	3	3.7	8.4	0.8
6 Oct 86					C				3	3.5	7.4	0.7
6 Oct 86						E			3.5	4.5	7.4	1.0
6 Oct 86								SE	3	4.4	9.6	0.8
13 Nov 86			NE						7	4.0	9.2	1.8
17 Nov 86						E			6	4.4	6.1	1.5
21 Nov 86					C				13	3.7	6.1	3.4
24 Nov 86								SE	3.5	3.5	9.2	1.0
3 Dec 86						E			3	4.0	9.8	0.8
6 Dec 86				W					4.5	3.5	8.1	1.2
7 Dec 86	NW								8	5.6	11.8	2.6
11 Dec 86					C				6.5	4.8	7.4	2.1
16 Dec 86				W					4	2.9	7.4	1.0
19 Dec 86							S		5.5	4.2	9.6	1.4
23 Dec 86					C				5.5	5.4	8.3	1.9
26 Dec 86								SE	3	4.0	12.5	0.7
1 Jan 87							S		4.5	3.3	6.3	1.0
1 Jan 87								SE	4	4.6	12.6	1.2
16 Jan 87						E			4	3.7	7.9	1.0
27 Jan 87								SE	10.5	4.1	8.7	2.3
7 Feb 87							S		6	4.6	10.7	1.7
7 Feb 87								SE	4	3.8	8.6	1.0
23 Feb 87					C				5.5	5.0	9.7	1.5
23 Feb 87						E			10	3.7	9.4	2.5
27 Feb 87							S		9.5	4.9	10.8	2.9
1 Mar 87								SE	8.5	6.3	12.0	2.8
3 Mar 87			NE						5	3.6	11.2	1.2
9 Apr 87				W					3.5	3.1	7.3	0.8
15 Apr 87							S		6.5	4.0	8.1	1.7

Table 1. (Continued)

Center Date	Classifying Region								Duration (Days)	Maximum Averaged Anomaly ($m\ s^{-1}$)	Maximum Point Anomaly ($m\ s^{-1}$)	Wind Measure (10^6 m)
	NW	N	NE	W	C	E	S	SE				
16 Apr 87								SE	11	5.4	10.6	3.2
17 Apr 87						E			12.5	3.6	9.1	2.9
22 Apr 87					C				8	3.9	9.3	2.0
26 Apr 87			NE						3.5	3.7	7.7	0.9
16 May 87			NE						3.5	3.0	8.5	0.8
19 May 87					C				14	5.5	8.1	4.5
27 May 87						E			3	2.6	6.7	0.6
30 May 87					C				3	3.3	8.1	0.7
5 Jul 87					C				3.5	3.2	6.9	0.7
10 Jul 87	NW								5	4.4	10.5	1.5
14 Jul 87							S		4	4.6	8.1	1.1
17 Jul 87								SE	5.5	4.3	7.8	1.3
18 Jul 87					C				15.5	4.7	8.5	4.1
29 Jul 87			NE						3.5	3.2	6.2	0.8
5 Aug 87						E			14	3.9	9.1	4.0
9 Sep 87		N							11.5	5.3	11.7	3.5
11 Sep 87	NW								8	3.4	10.6	2.0
18 Sep 87					C				3	3.6	8.9	0.8
25 Sep 87		N							5.5	4.4	8.3	1.6
9 Oct 87					C				3	3.1	7.5	0.7
19 Oct 87	NW								3.5	3.9	12.2	0.9
26 Oct 87						E			3	3.4	6.0	0.7
21 Nov 87				W					3	4.6	8.3	0.7
30 Nov 87						E			3.5	3.4	7.8	0.9
13 Dec 87			NE						4	6.3	13.9	1.3
18 Dec 87			NE						3.5	4.7	12.0	1.1
23 Dec 87							S		12	5.1	11.4	4.1
26 Dec 87								SE	7	4.9	8.5	2.2
8 Jan 88					C				13.5	5.7	11.1	4.1
11 Jan 88				W					5.5	3.7	8.3	1.3
22 Feb 88					C				3.5	3.5	6.0	0.9
23 Feb 88							S		15	5.7	14.2	4.3

Table 1. (Continued)

Center Date	Classifying Region								Duration (Days)	Maximum Averaged Anomaly ($m\ s^{-1}$)	Maximum Point Anomaly ($m\ s^{-1}$)	Wind Measure (10^6 m)
	NW	N	NE	W	C	E	S	SE				
1 Mar 88								SE	11.5	5.2	9.0	3.5
4 Apr 88							S		5.5	5.6	11.0	1.9
13 Apr 88							S		7.5	4.4	9.6	2.3
1 Jun 88	NW								4.5	3.2	7.4	1.1
28 Jul 88	NW								3.5	2.9	12.3	0.7
13 Dec 88	NW								4	3.3	11.3	1.0
2 Jan 89							S		8	3.9	14.3	2.0
10 Feb 89	NW								5.5	4.9	9.0	1.6
11 Feb 89			NE						3	3.0	10.1	0.7
2 Mar 89			NE						6.5	6.7	15.3	2.5
5 Mar 89	NW								4	3.4	6.2	1.0
19 Mar 89		N							5.5	5.2	10.2	1.9
22 Apr 89	NW								5.5	5.2	14.7	1.9
30 May 89							S		5	4.5	13.0	1.4
19 Jun 89	NW								5	3.7	10.4	1.1
31 Jul 89	NW								6	4.0	11.4	1.4
5 Aug 89	NW								3	2.8	10.7	0.6
8 Sep 89	NW								3.5	3.6	12.7	0.8
20 Oct 89				W					3	3.3	8.2	0.7
22 Nov 89		N							6	3.8	10.9	1.5
25 Nov 89				W					11	5.4	9.1	3.0
27 Nov 89							S		4	2.9	9.5	1.0
4 Dec 89	NW								9.5	4.0	11.8	2.7
6 Dec 89								SE	5.5	5.4	9.9	1.8
6 Dec 89				W					6	4.2	9.3	1.6
11 Dec 89			NE						4.5	3.7	12.0	1.1
16 Jan 90	NW								3.5	4.5	12.6	1.0
1 Feb 90							S		12.5	4.5	14.1	3.4
5 Feb 90					C				21.5	4.9	10.8	6.9
10 Feb 90								SE	9	5.5	12.0	2.9
12 Feb 90						E			3.5	5.9	11.6	1.3
16 Mar 90					C				5	6.7	14.0	1.7

Table 1. (Continued)

Center Date	Classifying Region								Duration (Days)	Maximum Averaged Anomaly ($m\ s^{-1}$)	Maximum Point Anomaly ($m\ s^{-1}$)	Wind Measure (10^6 m)
	NW	N	NE	W	C	E	S	SE				
17 Mar 90							S		9.5	4.8	14.4	2.4
23 Mar 90					C				4	3.8	7.6	1.0
29 Mar 90								SE	7	4.9	12.1	2.0
10 Jun 90							S		4	3.5	9.5	1.1
17 Jun 90				W					4.5	5.4	11.2	1.4
29 Jun 90		N							3	3.4	8.0	0.7
4 Jul 90				W					3	3.7	8.5	0.7
14 Jul 90		N							4	3.7	10.3	0.9
27 Jul 90	NW								5.5	3.7	6.6	1.2
14 Aug 90	NW								5	4.7	12.3	1.5
24 Aug 90					C				3	3.4	5.4	0.8
25 Aug 90	NW								4	3.1	12.1	0.9
12 Sep 90				W					4	3.4	8.4	0.9
5 Oct 90				W					3	2.9	6.1	0.6
7 Nov 90				W					5	3.2	8.6	1.1
15 Nov 90		N							5.5	3.9	10.5	1.5
17 Nov 90								SE	6.5	4.0	10.4	1.7
18 Nov 90							S		4.5	2.8	8.0	0.9
20 Nov 90				W					10.5	4.1	8.6	2.5
21 Nov 90					C				11	3.8	6.8	3.2
30 Nov 90		N							5	4.3	9.3	1.4
30 Nov 90	NW								9	4.8	15.5	2.2
1 Dec 90								SE	3.5	4.1	9.9	1.0
15 Dec 90					C				4.5	4.1	11.7	1.0
20 Dec 90				W					3.5	4.1	11.4	1.0
21 Dec 90	NW								5	4.2	15.7	1.3
26 Dec 90			NE						6.5	3.8	11.8	1.5
27 Dec 90					C				3	2.8	9.4	0.6
23 Feb 91							S		10.5	4.8	8.3	2.7
28 Feb 91					C				7	3.8	9.2	1.6
8 Mar 91				W					7.5	5.6	15.8	2.3
10 Mar 91							S		3.5	3.5	10.3	0.8

Table 1. (Continued)

Center Date	Classifying Region								Duration (Days)	Maximum Averaged Anomaly ($m\ s^{-1}$)	Maximum Point Anomaly ($m\ s^{-1}$)	Wind Measure (10^6 m)
	NW	N	NE	W	C	E	S	SE				
23 Mar 91		N							4.5	3.2	17.1	1.0
5 May 91				W					8	4.3	9.2	2.2
10 May 91						E			3	3.7	7.7	0.8
10 May 91	NW								3.5	2.7	11.2	0.7
11 May 91							S		5.5	5.1	17.0	1.7
11 May 91								SE	8	5.6	12.8	2.5
12 May 91					C				3	2.8	6.5	0.6
8 Jun 91							S		3	2.7	7.8	0.6
17 Jun 91					C				3.5	2.8	11.4	0.8
17 Jun 91	NW								6.5	4.1	11.8	1.9
22 Jun 91								SE	4.5	5.0	9.1	1.1
23 Jun 91						E			4.5	3.6	7.6	1.2
3 Jul 91			NE						3	2.9	6.0	0.6
27 Jul 91					C				4.5	3.1	7.5	0.9
27 Jul 91						E			3	3.2	7.5	0.7
2 Aug 91		N							3	3.3	6.3	0.6
10 Aug 91		N							8.5	4.8	9.4	2.8
11 Aug 91					C				5	4.1	8.7	1.3
14 Aug 91				W					5	3.2	7.0	1.1
17 Aug 91	NW								12	4.9	9.5	3.6
26 Aug 91	NW								3	3.0	9.0	0.6
6 Sep 91				W					10	3.9	9.7	2.5
10 Sep 91					C				5	2.5	7.5	1.0
13 Sep 91						E			7	3.2	8.4	1.5
13 Sep 91							S		3.5	3.5	9.3	0.9
13 Sep 91								SE	3	2.6	5.9	0.6
15 Sep 91			NE						6.5	3.4	9.8	1.6
21 Sep 91			NE						3	2.9	6.0	0.7
23 Sep 91					C				6	4.0	9.2	1.7
28 Sep 91				W					6	4.0	7.9	1.5
1 Oct 91						E			4.5	4.6	8.2	1.2
4 Oct 91	NW								4.5	3.2	12.6	1.1

Table 1. (Continued)

Center Date	Classifying Region								Duration (Days)	Maximum Averaged Anomaly ($m\ s^{-1}$)	Maximum Point Anomaly ($m\ s^{-1}$)	Wind Measure (10^6 m)
	NW	N	NE	W	C	E	S	SE				
17 Oct 91				W					4	3.7	7.3	0.9
23 Oct 91				W					3	3.5	10.1	0.8
24 Oct 91	NW								3.5	3.6	14.0	0.9
3 Nov 91					C				6.5	4.5	10.4	1.8
9 Nov 91						E			7	3.0	7.4	1.8
9 Nov 91	NW								9.5	5.1	22.9	3.0
13 Nov 91			NE						3.5	4.2	11.1	1.0
16 Nov 91					C				15.5	7.2	13.7	6.2
19 Nov 91						E			5	4.8	9.4	1.5
29 Nov 91			NE						5	5.6	11.0	1.6
29 Nov 91	NW								4	4.0	21.3	1.2
4 Dec 91						E			19	7.5	15.5	6.7
4 Dec 91							S		4.5	4.2	12.1	1.3
10 Dec 91								SE	12.5	8.2	21.2	5.1
12 Dec 91					C				12	3.6	10.6	2.9
27 Dec 91						E			4	2.7	6.1	0.8
1 Jan 92					C				12	6.0	9.5	5.2
8 Jan 92							S		7	5.8	19.4	2.1
11 Jan 92				W					5.5	5.7	11.0	1.8
14 Jan 92	NW								4.5	4.6	12.6	1.3
16 Jan 92					C				7	5.3	12.6	2.0
19 Jan 92						E			23	8.2	13.8	11.5
19 Jan 92							S		3	3.0	10.1	0.7
19 Jan 92								SE	15	8.5	15.0	7.1
4 Feb 92								SE	7	4.3	11.4	1.8
9 Feb 92						E			6.5	4.8	10.1	2.0
11 Feb 92			NE						5.5	4.2	9.7	1.3
22 Feb 92						E			4	2.6	5.6	0.8
3 Mar 92								SE	3.5	3.0	8.4	0.8
8 Mar 92					C				4	3.8	10.1	1.1
10 Mar 92						E			8	2.7	9.1	1.8
10 Mar 92							S		24.5	5.3	14.7	7.8

Table 1. (Continued)

Center Date	Classifying Region								Duration (Days)	Maximum Averaged Anomaly ($m\ s^{-1}$)	Maximum Point Anomaly ($m\ s^{-1}$)	Wind Measure (10^6 m)
	NW	N	NE	W	C	E	S	SE				
17 Mar 92								SE	19	7.6	16.5	6.8
23 Mar 92						E			10.5	6.2	10.9	4.0
8 Apr 92						E			3.5	4.7	8.9	1.0
21 Apr 92							S		5	6.1	15.2	1.8
22 Apr 92					C				5.5	4.4	10.3	1.6
22 Apr 92								SE	3.5	5.4	19.2	1.1
25 Apr 92			NE						3	3.2	6.6	0.7
26 Apr 92						E			7	6.3	12.2	2.4
14 May 92					C				4	2.7	9.1	0.9
14 May 92			NE						3	2.8	8.6	0.6
15 May 92						E			7	3.9	7.4	1.9
19 May 92					C				4	2.9	7.0	0.9
26 Jun 92					C				3	3.7	6.5	0.7
4 Jul 92						E			5	2.9	7.2	1.1
7 Jul 92			NE						9	3.8	8.5	2.2
9 Jul 92						E			4.5	3.2	6.9	1.0
12 Aug 92			NE						4.5	3.4	8.4	0.9
16 Aug 92	NW								3	2.8	12.4	0.6
8 Sep 92						E			3	2.8	5.3	0.6
8 Sep 92	NW								4.5	3.5	10.5	1.0
9 Sep 92		N							11.5	5.9	20.4	4.5
10 Sep 92					C				4	3.6	7.3	1.0
10 Sep 92			NE						8	5.3	12.3	2.4
14 Sep 92	NW								4	2.9	9.5	0.9
16 Sep 92								SE	4	2.7	8.0	0.9
17 Sep 92							S		5.5	3.6	7.7	1.5
20 Sep 92					C				4	4.4	7.6	1.0
13 Oct 92								SE	4.5	4.1	9.7	1.4
15 Oct 92	NW								4	3.1	9.8	0.9
22 Oct 92	NW								6.5	4.8	20.4	1.9
25 Oct 92					C				3	2.9	9.1	0.6
27 Oct 92				W					3	3.2	7.1	0.7

Table 1. (Continued)

Center Date	Classifying Region								Duration (Days)	Maximum Averaged Anomaly ($m\ s^{-1}$)	Maximum Point Anomaly ($m\ s^{-1}$)	Wind Measure (10^6 m)
	NW	N	NE	W	C	E	S	SE				
31 Oct 92		N							3	4.3	12.6	0.8
10 Nov 92						E			4	4.5	11.9	1.2
19 Nov 92			NE						4	5.6	14.4	1.2
20 Nov 92	NW								10	4.4	12.1	3.0
25 Nov 92			NE						3	5.4	13.0	0.9
29 Nov 92						E			4	2.8	11.5	0.8
9 Dec 92		N							3	3.9	15.7	0.8
1 Jan 93							S		8.5	10.4	19.3	3.8
2 Jan 93					C				11.5	6.4	14.8	4.2
3 Jan 93								SE	7	4.4	14.0	2.5
5 Jan 93			NE						9.5	4.0	14.8	2.5
27 Jan 93	NW								4	3.5	15.3	0.9
29 Jan 93				W					4.5	3.9	11.3	1.3
31 Jan 93					C				10	5.0	11.0	2.5
6 Feb 93								SE	12	6.2	15.1	4.0
10 Feb 93					C				4.5	3.7	9.5	1.2
9 Mar 93					C				8	5.1	11.0	2.3
13 Mar 93				W					3	2.9	10.2	0.7
15 Mar 93							S		10	3.3	13.1	2.4
16 Mar 93	NW								4	3.6	11.3	1.1
16 Apr 93					C				5	4.2	10.0	1.4
14 May 93						E			3.5	4.2	8.2	1.0
15 May 93				W					3	3.1	6.8	0.6
12 Jul 93								SE	4.5	3.1	7.1	1.0
2 Aug 93				W					3.5	3.5	10.0	0.8
13 Aug 93					C				8	3.8	9.5	2.0
17 Aug 93			NE						5	4.1	10.2	1.2
19 Aug 93		N							4.5	4.5	11.2	1.3
22 Aug 93						E			3	2.9	7.3	0.6
23 Aug 93	NW								3.5	3.1	10.2	0.8
29 Aug 93								SE	3	3.8	9.6	0.8
23 Sep 93	NW								3	4.1	12.9	0.8

Table 1. (Continued)

Center Date	Classifying Region								Duration (Days)	Maximum Averaged Anomaly ($m\ s^{-1}$)	Maximum Point Anomaly ($m\ s^{-1}$)	Wind Measure (10^6 m)
	NW	N	NE	W	C	E	S	SE				
11 Oct 93					C				5	5.3	12.0	1.3
20 Oct 93		N							11	6.1	16.8	3.2
22 Oct 93								SE	5	4.1	13.1	1.1
25 Oct 93					C				7	5.1	12.3	1.9
25 Oct 93						E			3	3.6	8.8	0.8
26 Oct 93			NE						8	4.3	15.8	2.0
6 Jan 94							S		6.5	3.2	9.1	1.5
10 Jan 94								SE	4	3.7	10.5	1.0
16 Feb 94			NE						5.5	4.0	10.3	1.4
22 Feb 94				W					4.5	4.0	11.2	1.1
21 Mar 94					C				4.5	4.8	13.0	1.3
5 Apr 94	NW								3.5	2.4	8.9	0.7
14 Apr 94					C				4	4.1	10.1	1.1
25 Apr 94								SE	3.5	4.5	9.3	0.9
10 May 94				W					6	4.8	11.2	2.0
15 May 94	NW								5.5	5.2	16.8	1.9
7 Jul 94	NW								3.5	3.2	13.8	0.8
15 Jul 94	NW								5	3.3	9.9	1.1
18 Jul 94								SE	7	4.7	14.1	1.8
24 Jul 94				W					4	3.9	9.5	1.1
26 Jul 94	NW								8	4.4	11.8	2.5
2 Aug 94								SE	3	4.6	12.3	0.9
10 Aug 94					C				5	3.2	8.2	1.2
15 Aug 94				W					5.5	3.4	9.8	1.2
27 Aug 94					C				4.5	3.0	7.2	1.1
28 Aug 94								SE	3	3.7	13.6	0.8
4 Sep 94				W					8	3.0	9.4	1.7
11 Sep 94					C				7.5	4.7	11.5	2.2
19 Sep 94							S		5	4.0	10.8	1.2
23 Sep 94	NW								13	4.8	14.1	4.0
23 Sep 94								SE	8	5.5	10.7	2.2
24 Sep 94						E			4.5	6.9	10.6	1.7

Table 1. (Continued)

Center Date	Classifying Region								Duration (Days)	Maximum Averaged Anomaly ($m\ s^{-1}$)	Maximum Point Anomaly ($m\ s^{-1}$)	Wind Measure (10^6 m)
	NW	N	NE	W	C	E	S	SE				
25 Sep 94			NE						15.5	6.2	11.0	5.5
29 Sep 94		N							32.5	7.4	13.9	10.5
6 Oct 94						E			5	5.2	9.0	1.5
14 Oct 94					C				10.5	4.5	9.1	3.0
20 Oct 94		N							6.5	4.9	11.7	1.9
21 Oct 94			NE						9.5	4.9	12.0	2.8
25 Oct 94	NW								11.5	7.0	17.4	3.9
30 Oct 94		N							15	6.4	11.4	4.6
1 Nov 94			NE						8	5.7	12.1	2.8
3 Nov 94						E			8	3.7	7.9	2.2
9 Nov 94						E			3	2.8	6.8	0.6
12 Nov 94					C				18	6.9	11.9	6.5
17 Nov 94		N							5.5	4.3	9.6	1.6
19 Nov 94								SE	3.5	2.8	8.7	0.7
24 Nov 94		N							3.5	3.1	8.3	0.8
13 Dec 94					C				15.5	5.6	9.5	5.2
21 Dec 94		N							3	4.4	14.0	0.8
23 Dec 94	NW								4	3.2	15.2	0.9
25 Dec 94					C				6	6.0	11.5	1.9
2 Jan 95								SE	8.5	5.1	14.2	2.9
29 Jan 95			NE						3	3.4	9.8	0.7
8 Feb 95								SE	3	3.1	7.7	0.7
4 Mar 95			NE						4.5	4.2	10.8	1.1
10 Mar 95							S		3	3.8	10.7	0.7
20 Apr 95							S		9.5	3.8	8.6	2.4
29 Apr 95					C				4.5	4.3	15.1	1.2
22 May 95	NW								4	4.3	9.0	1.1
25 May 95							S		5	3.9	10.3	1.3
28 May 95								SE	3.5	5.2	10.6	1.1
1 Dec 95								SE	5.5	3.6	8.1	1.3
18 Dec 95								SE	11	6.2	13.4	3.5
21 Dec 95							S		9	3.3	9.3	2.1

Table 2. Duration, Maximum Averaged Anomaly, Wind Measure and Maximum Point Anomaly for each composite WWE. Quantities as defined in Section 3.a.

Region	Duration (days)	Maximum Averaged Anomaly (m s^{-1})	Wind Measure (10^6 m)	Maximum Point Anomaly (m s^{-1})
NW	5	4.0	1.3	7.2
N	5.5	4.6	1.6	6.6
NE	4	4.2	1.1	6.3
W	4.5	3.9	1.1	6.9
C	5.5	4.4	1.4	6.4
E	4.5	4.1	1.2	5.5
S	5	4.4	1.4	6.4
SE	5	4.7	1.4	6.7

Table 3. Table of scales for the composite WWEs according to the simple Gaussian model described in section 4.b.

Region	U_o (m s^{-1})	X_o	Y_o	L_x (10^6 m)	L_y (10^6 m)	T (days)	c_x (m s^{-1})	c_y (m s^{-1})
NW	7.2	132.5°E	12.5°N	1.4	0.6	3.5	–3.8	2.6
N	6.6	165°E	10°N	2.5	0.7	3	–5.1	0.3
NE	6.3	165°W	12.5°N	1.6	1.1	2.5	1.3	
W	6.9	142.5°E	0°	1.7	0.4	3.5	–1.3	1.3
C	6.4	170°E	0°	1.8	0.6	3		
E	5.5	172.5°W	2.5°S	1.9	0.7	3	–1.3	
S	6.4	170°E	10°S	2.2	0.7	2.5	2.5	
SE	6.7	167.5°W	10°S	1.6	0.7	3.5	3.8	

Table 4. Table of WWEs occurring during the TOGA-COARE IOP (Nov 1992–Feb 1993). Quantities are as defined in Section 3.1. Highlighted in bold italics are the events whose wind measure statistic is greater than or equal to 2.5×10^6 m.

Region	Date	Maximum Point Anomaly ($m\ s^{-1}$)	Duration (days)	Maximum Averaged Anomaly ($m\ s^{-1}$)	Measure (10^6 m)
N	31 Oct 92	12.6	3	4.3	0.8
E	10 Nov 92	11.9	4	4.5	1.2
NE	19 Nov 92	14.4	4	5.6	1.2
NW	***20 Nov 92***	***12.1***	***10***	***4.4***	***3***
NE	25 Nov 92	13	3	5.4	0.9
E	29 Nov 92	11.5	4	2.8	0.8
N	9 Dec 92	15.7	3	3.9	0.8
S	***1 Jan 93***	***19.3***	***8.5***	***10.4***	***3.8***
C	***2 Jan 93***	***14.8***	***11.5***	***6.4***	***4.2***
SE	***3 Jan 93***	***14***	***7***	***4.4***	***2.5***
NE	***5 Jan 93***	***14.8***	***9.5***	***4***	***2.5***
NW	27 Jan 93	15.3	4	3.5	0.9
W	29 Jan 93	11.3	4.5	3.9	1.3
C	***31 Jan 93***	***11***	***10***	***5***	***2.5***
SE	***6 Feb 93***	***15.1***	***12***	***6.2***	***4***
C	10 Feb 93	9.5	4.5	3.7	1.2

FIGURES

(The eight figures below are included as samples. Please refer to the printed report for the complete set of figures.)

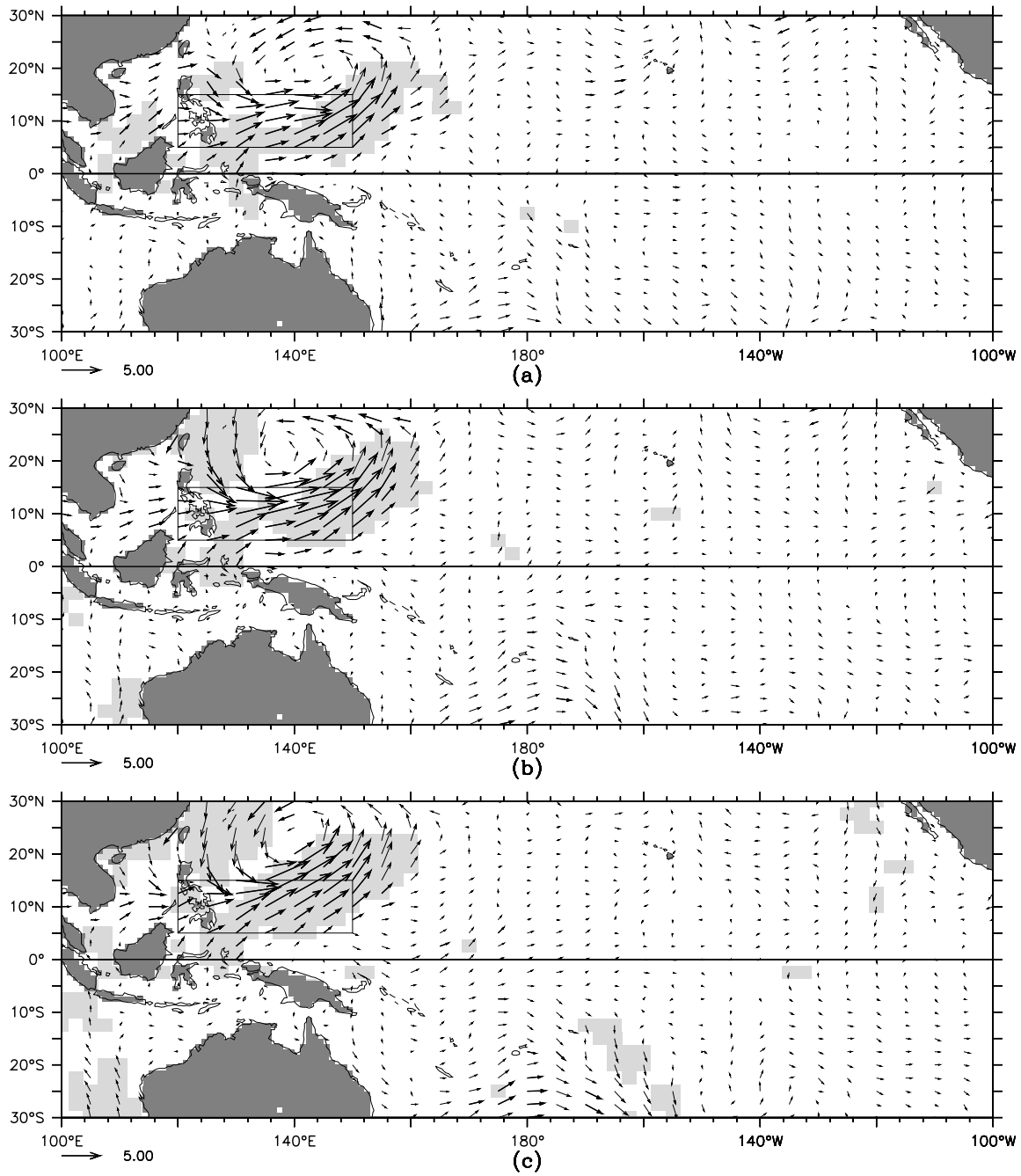

Fig. 35. Type NW composite WWE 10-m wind anomaly vector map, for (a) day(–1), (b) day(0) and (c) day(1). The classifying region is indicated by the thin lined box. The scale vector is 5 m s^{-1}. Zonal wind anomalies statistically significant at 99% are indicated by bold vectors, meridional wind anomalies significant at 99% are indicated by shaded background. Significance is determined as described in the Appendix.

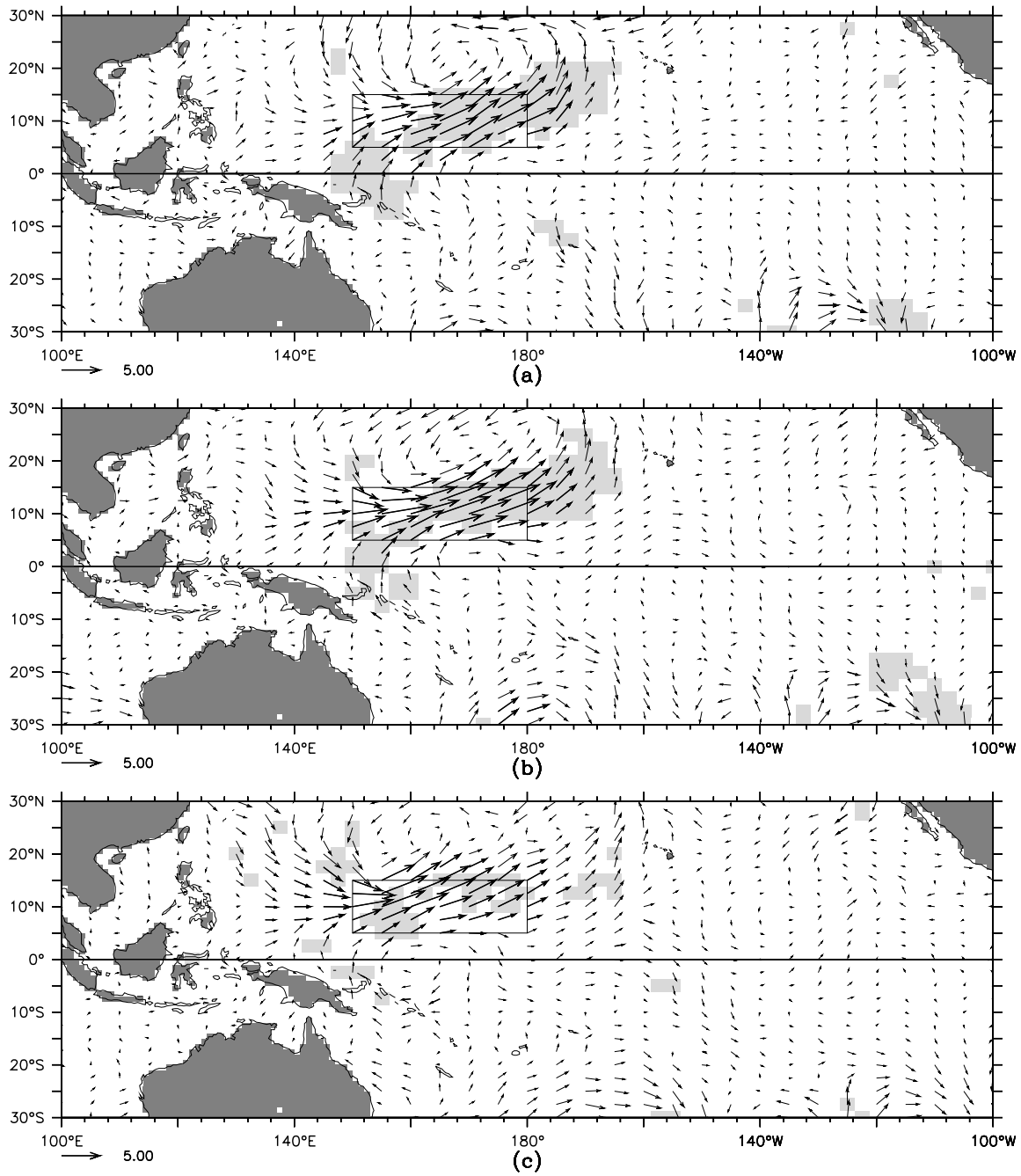

Fig. 42. Type N composite WWE 10-m wind anomaly vector map, for (a) day(–1), (b) day(0) and (c) day(1). The classifying region is indicated by the thin lined box. The scale vector is 5 m s^{-1}. Zonal wind anomalies statistically significant at 99% are indicated by bold vectors, meridional wind anomalies significant at 99% are indicated by shaded background. Significance is determined as described in the Appendix.

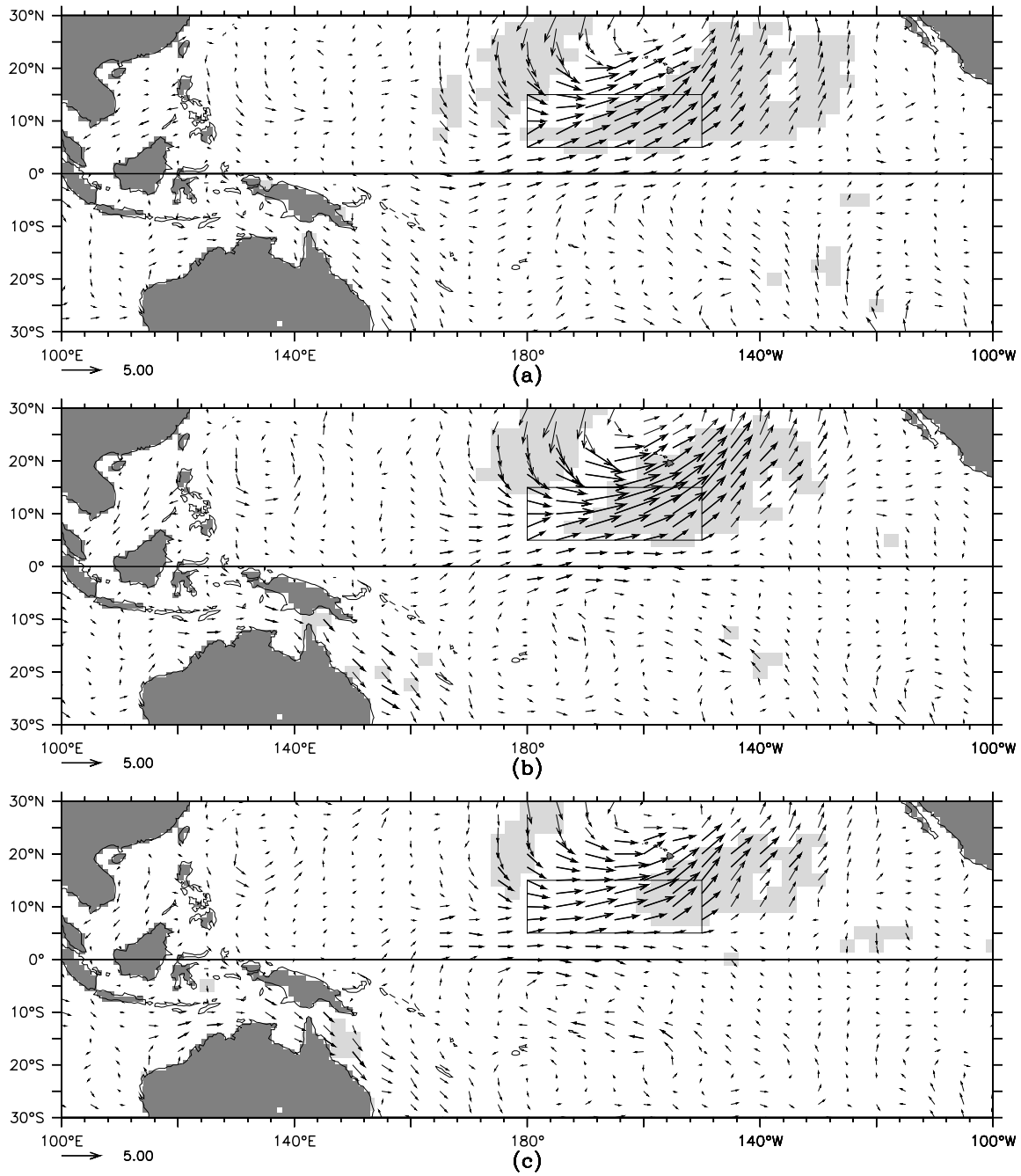

Fig. 49. Type NE composite WWE 10-mr wind anomaly vector map, for (a) day(–1), (b) day(0) and (c) day(1). The classifying region is indicated by the thin lined box. The scale vector is 5 m s^{-1}. Zonal wind anomalies statistically significant at 99% are indicated by bold vectors, meridional wind anomalies significant at 99% are indicated by shaded background. Significance is determined as described in the Appendix.

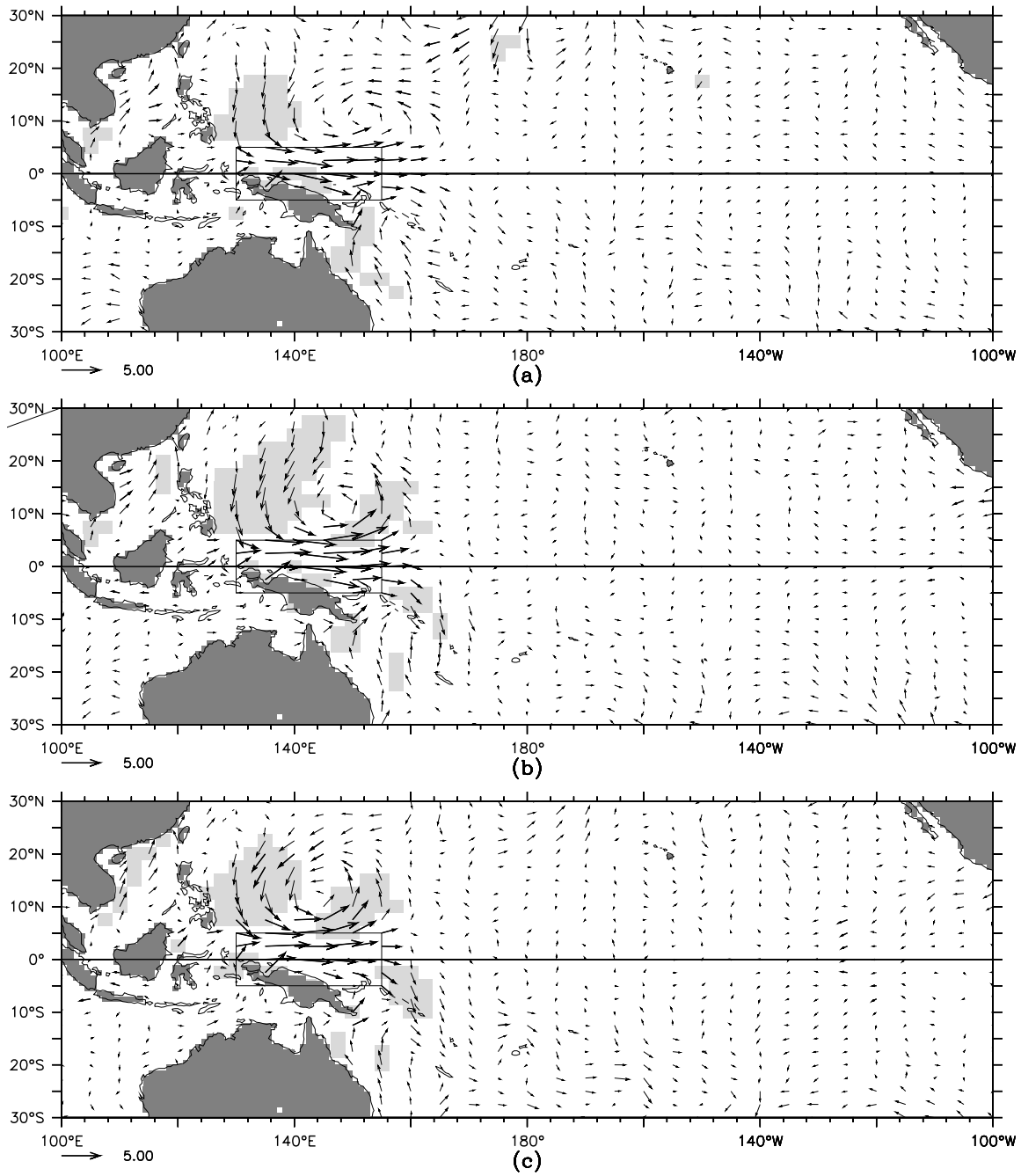

Fig. 56. Type W composite WWE 10-m wind anomaly vector map, for (a) day(–1), (b) day(0) and (c) day(1). The classifying region is indicated by the thin lined box. The scale vector is 5 m s^{-1}. Zonal wind anomalies statistically significant at 99% are indicated by bold vectors, meridional wind anomalies significant at 99% are indicated by shaded background. Significance is determined as described in the Appendix.

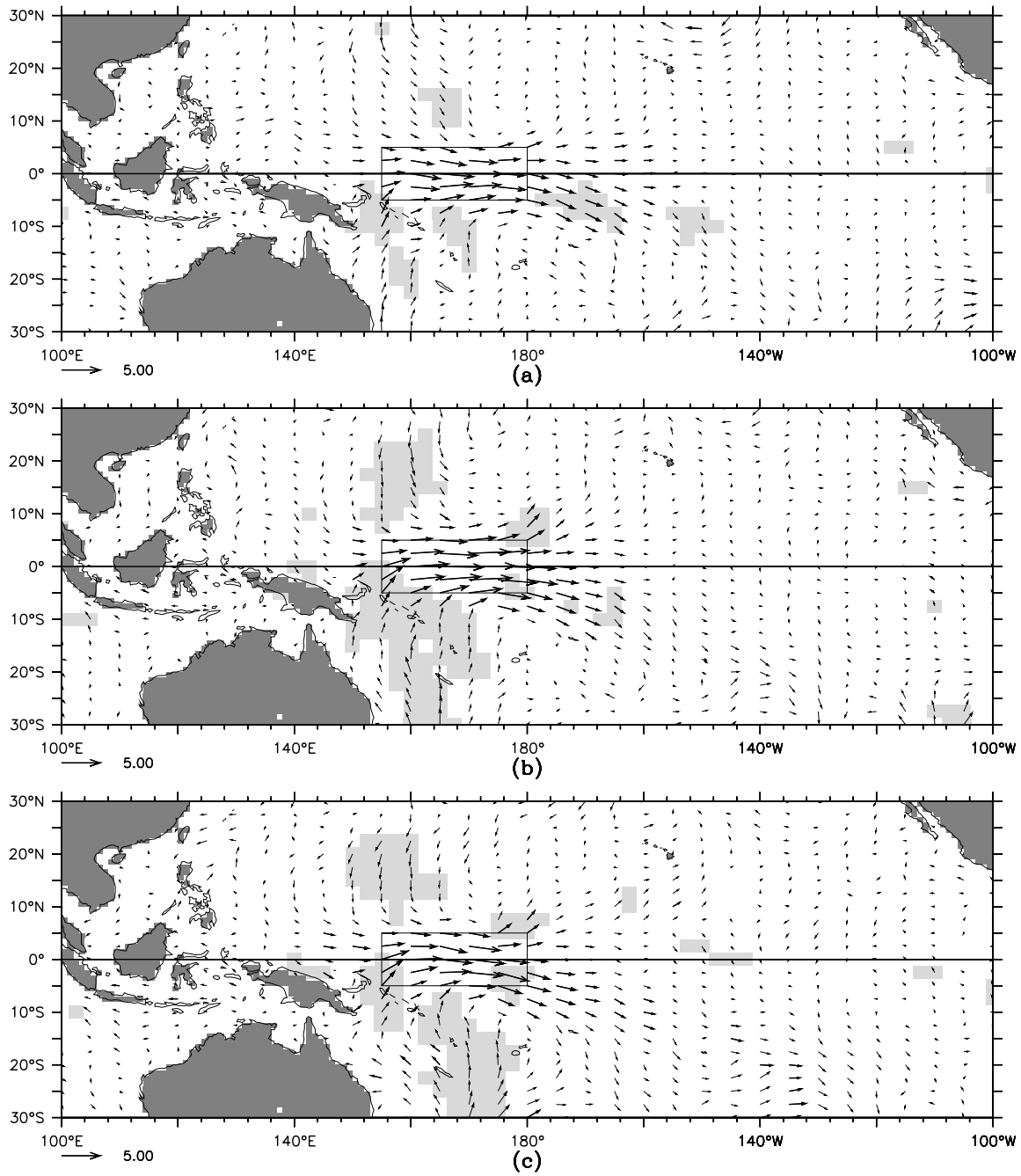

Fig. 63. Type C composite WWE 10-m wind anomaly vector map, for (a) day(–1), (b) day(0) and (c) day(1). The classifying region is indicated by the thin lined box. The scale vector is 5 m s^{-1}. Zonal wind anomalies statistically significant at 99% are indicated by bold vectors, meridional wind anomalies significant at 99% are indicated by shaded background. Significance is determined as described in the Appendix.

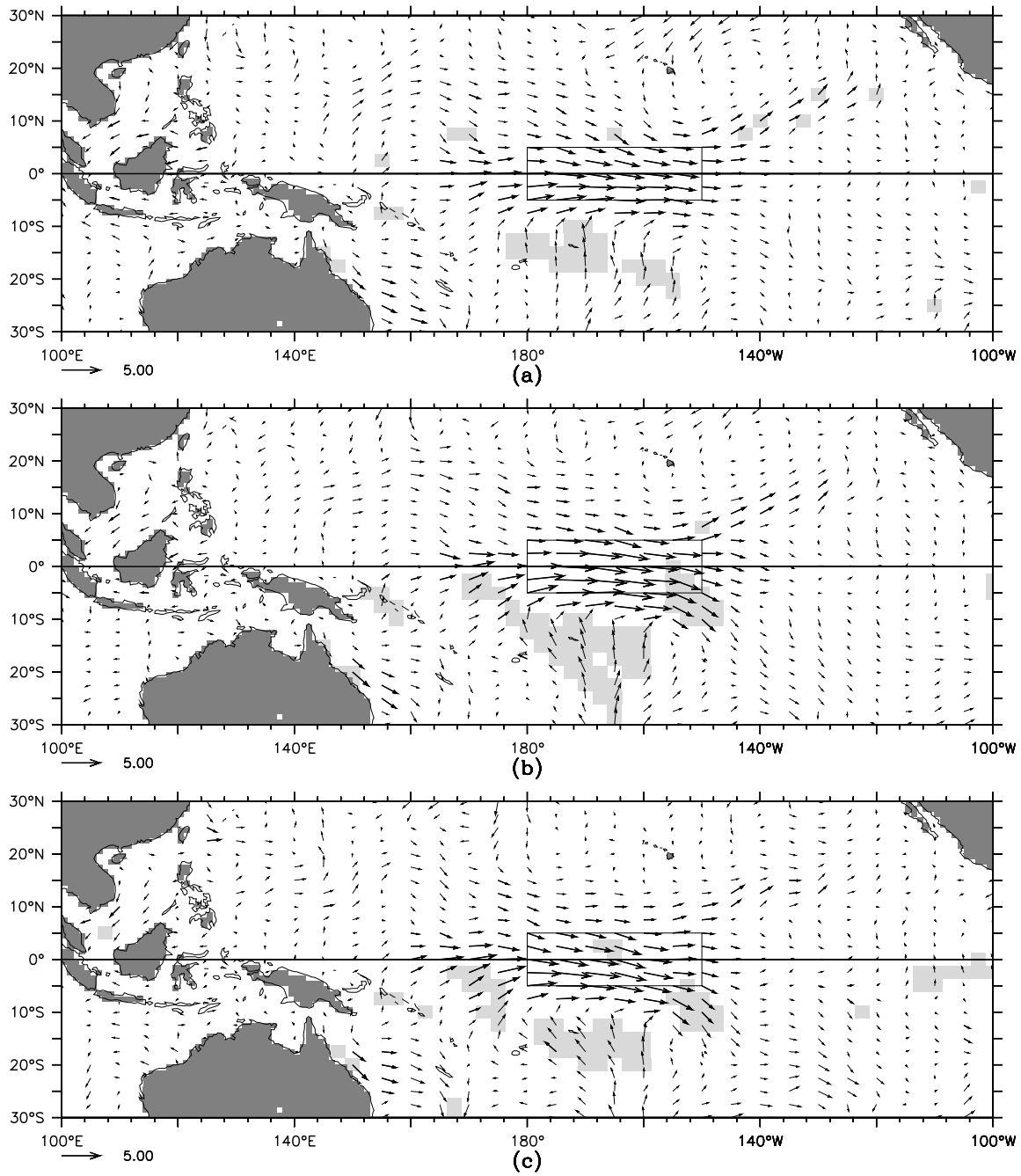

Fig. 70. Type E composite WWE 10-m wind anomaly vector map, for (a) day(–1), (b) day(0) and (c) day(1). The classifying region is indicated by the thin lined box. The scale vector is 5 m s^{-1}. Zonal wind anomalies statistically significant at 99% are indicated by bold vectors, meridional wind anomalies significant at 99% are indicated by shaded background. Significance is determined as described in the Appendix.

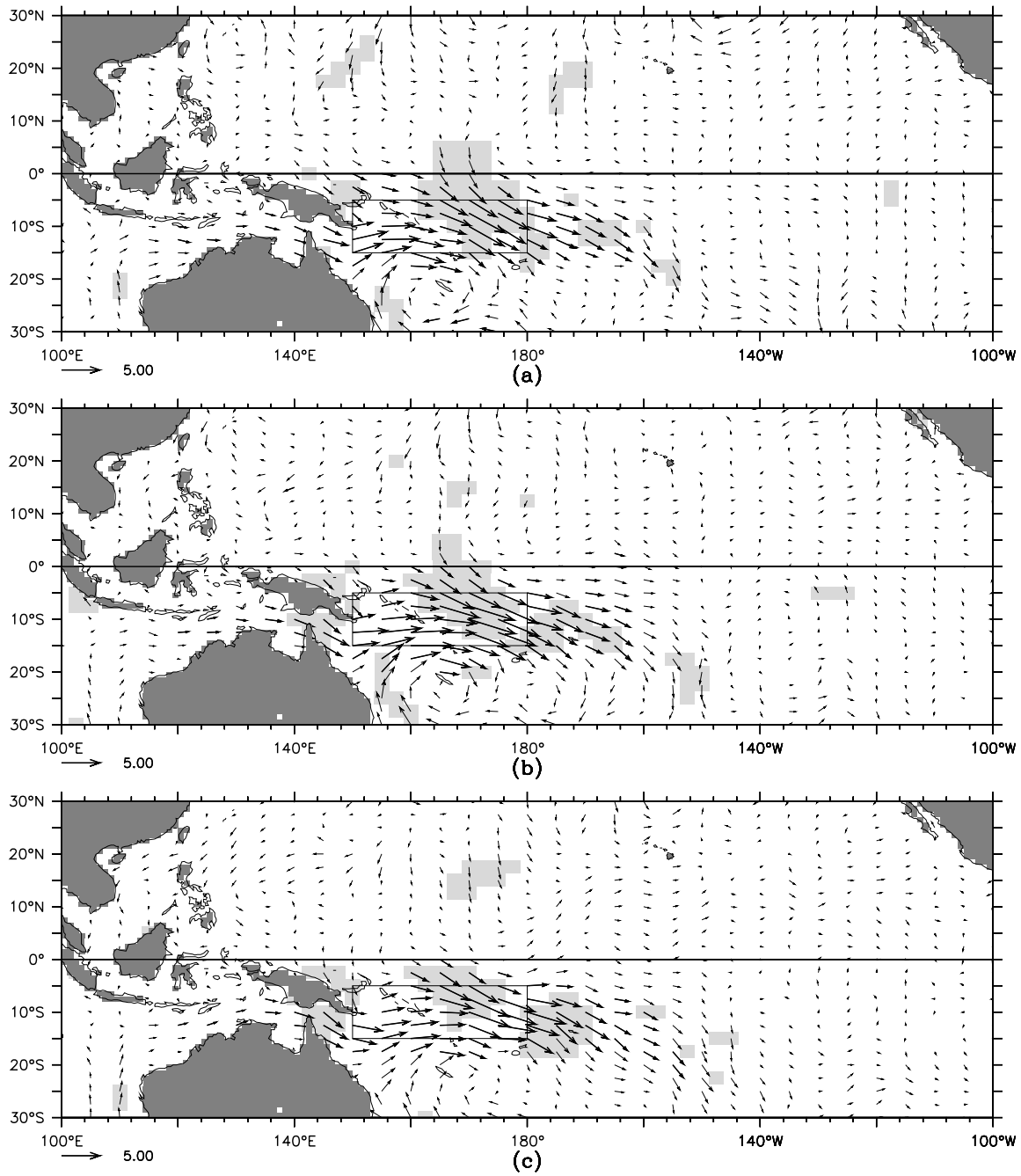

Fig. 77. Type S composite WWE 10-m wind anomaly vector map, for (a) day(–1), (b) day(0) and (c) day(1). The classifying region is indicated by the thin lined box. The scale vector is 5 m s^{-1}. Zonal wind anomalies statistically significant at 99% are indicated by bold vectors, meridional wind anomalies significant at 99% are indicated by shaded background. Significance is determined as described in the Appendix.

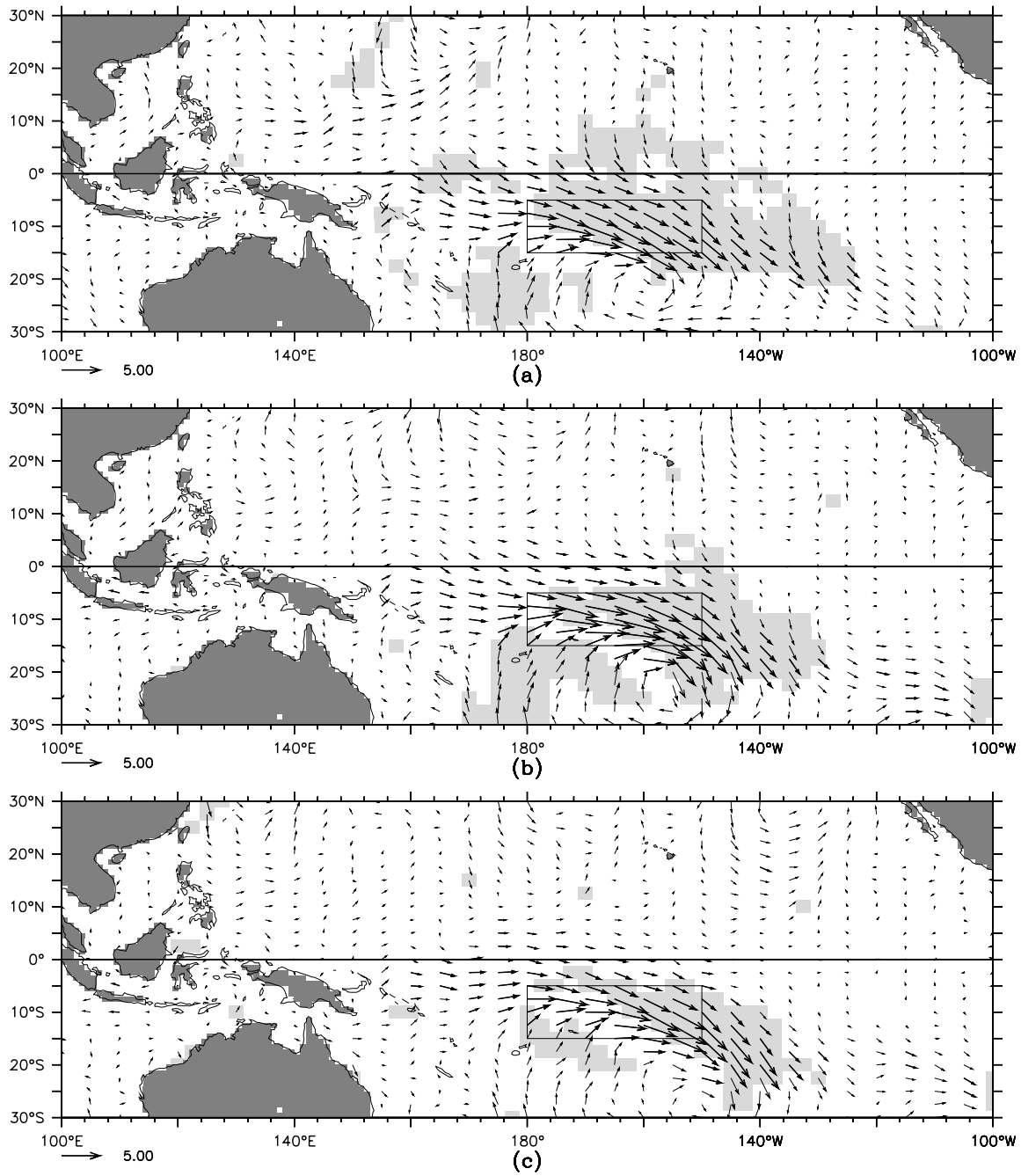

Fig. 84. Type SE composite WWE 10-m wind anomaly vector map, for (a) day(–1), (b) day(0) and (c) day(1). The classifying region is indicated by the thin lined box. The scale vector is 5 m s^{-1}. Zonal wind anomalies statistically significant at 99% are indicated by bold vectors, meridional wind anomalies significant at 99% are indicated by shaded background. Significance is determined as described in the Appendix.

Westerly Wind Event (WWE) Web Page

This page includes interactive access to figures of the wind anomalies and the winds for the eight different types of composite events, along with animated gifs of the winds and wind anomalies.

http://dread.pmel.noaa.gov/~gabe/wwe/wwemain.html